Mitochondrial Function is Preserved Under Cysteine Starvation via Glutathione Catabolism in NSCLC

Nathan P. Ward[1][*], Sang Jun Yoon[1], Tyce Flynn[1], Amanda Sherwood[1], Juliana Madej[1], Gina M. DeNicola[1][*]

[1]Department of Cancer Physiology, Moffitt Cancer Center
*Correspondence to: gina.denicola@moffitt.org; nathan.ward@moffitt.org

Abstract

Cysteine metabolism occurs across cellular compartments to support diverse biological functions and prevent the induction of ferroptosis. Though the disruption of cytosolic cysteine metabolism is implicated in this form of cell death, it is unknown whether the substantial cysteine metabolism resident within the mitochondria is similarly pertinent to ferroptosis. Here, we show that despite the rapid depletion of intracellular cysteine upon loss of extracellular cystine, cysteine-dependent synthesis of Fe-S clusters persists in the mitochondria of lung cancer cells. This promotes a retention of respiratory function and a maintenance of the mitochondrial redox state. Under these limiting conditions, we find that mitochondrial glutathione sustains the function of the Fe-S proteins critical to oxidative metabolism. This is achieved through CHAC1 catabolism of the cysteine-containing tripeptide within the mitochondrial matrix. We find that disrupting Fe-S cluster synthesis under cysteine restriction protects against the induction of ferroptosis, suggesting that the preservation of mitochondrial function is antagonistic to survival under starved conditions. Overall, our findings implicate mitochondrial cysteine metabolism in the induction of ferroptosis and reveal a novel mechanism of mitochondrial resilience in response to nutrient stress.

Main

The proteinogenic amino acid cysteine (Cys) is a significant contributor to cellular functions due to its resident thiol group. Cysteine supplies this reactive sulfur in support of cellular antioxidant capacity (glutathione [GSH]), electron transfer (iron-sulfur [Fe-S] clusters), energy metabolism (coenzyme A), and osmoregulation (taurine)[1]. Despite the essentiality of cysteine for these processes, there is an apparent therapeutic window in restricting cysteine systemically as an anti-cancer strategy[2,3]. Indeed, cysteine becomes conditionally essential across many tumor species[4], in part due to an inability to synthesize the amino acid from methionine through the transsulfuration pathway[5]. This dictates a reliance on an extracellular source of cysteine, predominantly in its oxidized form of cystine (Cys_2). Cysteine availability can be targeted through its systemic depletion[2] or inhibition of the primary Cys_2 transporter, system X_c^-[6].

Cysteine restriction promotes an iron-dependent form of cell death known as ferroptosis[7], where Fenton chemistry promotes the generation of free radicals that initiate lipid radical formation and the unsustainable peroxidation of plasma membrane phospholipids[8]. The resulting loss of membrane integrity is suppressed by intrinsic pathways mediated by ferroptosis suppressor protein 1 (FSP1)[9] and glutathione peroxidase 4 (GPX4)[10] to ward off ferroptosis under basal conditions. However, in the absence of cysteine, cancer cells are unable to synthesize GSH, restricting GPX4 activity and inducing ferroptosis.

53   Additional factors have been implicated in the induction of ferroptosis[11], including the

54   engagement of mitochondrial metabolism and the tricarboxylic acid (TCA) cycle[12,13].

55   Mechanisms by which the TCA cycle promotes ferroptosis include the generation and

56   export of citrate to drive the synthesis of new substrates for lipid peroxidation[14], and the

57   stimulation of the electron transport chain (ETC)[13]. However, how ETC activity promotes

58   the induction of ferroptosis remains to be fully elucidated[15]. Existing evidence suggests

59   that ATP production[14] and the generation and extramitochondrial release of reactive

60   oxygen species (ROS) may be relevant consequences[15,16].

61

62   One aspect of mitochondrial metabolism that has not been adequately addressed is the

63   role of resident cysteine metabolism within the mitochondria. Though the disruption of

64   cytosolic cysteine metabolism (i.e., GSH synthesis) plays a significant role in the induction

65   of ferroptosis under cysteine limitation[5,17], it remains unknown if alterations in

66   mitochondrial cysteine metabolism are also operative. Mitochondrial cysteine is used in

67   the synthesis of mitochondrially encoded protein components of the ETC, hydrogen

68   sulfide production[18], and Fe-S cluster synthesis[19] in support of bioenergetic metabolism.

69   Given the established connection between oxidative metabolism and ferroptosis[12,13], the

70   requirement for cysteine in support of respiration suggests it may be particularly relevant

71   to ferroptosis. Furthermore, a disruption in mitochondrial cysteine metabolism could

72   explain the gradual loss of mitochondrial function reportedly associated with prolonged

73   cysteine deprivation[3,13,20,21].

74

75 To interrogate the influence of mitochondrial cysteine metabolism in the induction of

76 ferroptosis, we evaluated mitochondrial respiratory function in response to prolonged

77 cysteine deprivation with regard to the capacity for Fe-S cluster synthesis. We evaluated

78 this in the context of non-small cell lung cancer (NSCLC), given their sensitivity to cysteine

79 starvation[22] and the robust mitochondrial metabolism exhibited by human lung

80 tumors[23,24]. Remarkably, despite the rapid depletion of mitochondrial cysteine under

81 starved conditions, Fe-S cluster synthesis persisted in support of respiratory function

82 through the onset of ferroptosis. This was achieved through the catabolism of

83 mitochondrial GSH and at the expense of NSCLC viability.

84

85 **Results**

86

87 Mitochondrial Respiratory Function Persists Under Cystine Deprivation

88 To determine the influence of cysteine deprivation on mitochondrial metabolism, we

89 restricted extracellular cystine in a panel of NSCLC cells. We opted to starve cells of their

90 source of cysteine rather than inhibit cystine uptake with erastin to directly assess the

91 consequences of cysteine deprivation without the confounding influence of erastin's

92 promiscuous inhibition of the mitochondrial voltage-dependent anion channel[25,26]. As

93 previously described, NSCLC cells succumb to ferroptosis in the absence of cysteine[5,27]

94 (**Extended Data Figure 1a-c**). We begin to observe the accumulation of ferroptotic cells,

95 as detected upon the intercalation of a cell-impermeable fluorescent dye with nuclear

96 DNA, following 24h of cystine deprivation (**Extended Data Figure 1a**). Therefore, we

97   performed our mitochondrial analyses upon 20h of starvation to ensure sufficient nutrient

98   stress in the absence of a loss of cell viability.

99

100   To assess general mitochondrial respiratory function under cystine deprivation, we

101   employed the Seahorse MitoStress test. Generally, the basal oxygen consumption rate

102   (OCR) of NSCLC cells was not diminished in the absence of cystine (**Figure 1a**),

103   indicating a retention of mitochondrial respiration. This coincided with a maintenance of

104   mitochondrial coupling efficiency (**Figure 1b**), an indicator of the functionality of the

105   mitochondrial inner membrane (IMM)[28]. Further, though it was reported that the IMM

106   becomes dramatically hyperpolarized under cysteine deprivation[13], mitochondrial

107   membrane potential ($\Delta\Psi_m$) was either minimally increased or unchanged under starved

108   conditions (**Figure 1c**). Consistent with the preservation of a functional IMM, ATP-linked

109   respiration was not compromised in the absence of cystine (**Figure 1d**). Moreover,

110   several NSCLC lines exhibited a significant elevation in maximal respiratory capacity that

111   could not be explained by an increase in mitochondrial density (**Figures 1e and 1f**),

112   suggesting that cysteine deprivation may enhance mitochondrial function beyond the

113   requirement for oxidative phosphorylation. Collectively, these data indicate a robust

114   persistence of mitochondrial respiration under cystine deprivation that occurs

115   independent of an expected insult to the IMM[13,20].

116

117   <u>Cystine Deprivation Does Not Promote Mitochondrial Oxidative Stress</u>

118   To confirm that the persistence of respiratory function is not damaging to the mitochondria

119   of NSCLC cells, we interrogated the mitochondrial redox state in response to cystine

120   starvation. First, we employed a series of fluorescent ROS indicators to assess changes

121   in the mediators of oxidative stress. While we observe the hallmark increase in lipid

122   peroxidation at the cellular level (**Figure 2a**)[8], and a coincident increase in cellular free

123   radical levels under cystine deprivation (**Figure 2b**), these indications of oxidative stress

124   do not extend to the mitochondria. Use of specific and mitochondrially targeted indicators

125   of superoxide ($\bullet O_2^-$) and hydrogen peroxide (H_2O_2) revealed that prolonged cystine

126   starvation did not alter the abundance of either species (**Figures 2c and 2d**). This

127   suggests that cysteine deprived mitochondria can scavenge the significant ROS

128   generated as a byproduct of persistent mitochondrial metabolism[29].

129

130   Mitochondrial ROS metabolism is achieved predominantly through the activity of two

131   complementary, yet distinct thiol-based antioxidant systems[30]. Both the GSH tripeptide

132   and the small molecular weight protein thioredoxin (TXN) support ROS detoxification by

133   a network of antioxidant proteins within the mitochondria[31]. Through use of a genetically

134   encoded and mitochondrially targeted biosensor[32], we determined that the mitochondrial

135   GSH pool was more reduced under cystine deprivation relative to replete conditions

136   (**Figure 2e**). Further, an assessment of the oxidation state of peroxiredoxin 3 (PRDX3),

137   a component of the TXN system, revealed an increase in the functional reduced form

138   upon cystine starvation (**Figure 2f**). Together these data suggest that cystine deprivation

139   elicits a more reduced mitochondrial matrix despite robust metabolic activity. In

140   agreement with this apparent lack of oxidative stress, we did not observe mitochondrial

141   lipid peroxidation upon cystine deprivation (**Figure 2g**), which indicates the increase in

142   whole cell lipid peroxidation is confined to the plasma membrane (**Figure 2a**).

143   Collectively, these data reflect that a maintenance of mitochondrial redox homeostasis

144   accompanies the persistence of respiration in cysteine restricted NSCLC cells.

145

146   Fe-S Cluster Synthesis is Sustained Under Cystine Deprivation

147   Cysteine is a requirement for sustained mitochondrial function, due in large part to its

148   utilization in the synthesis of Fe-S clusters. These redox cofactors mediate electron

149   transfer and support the enzymatic function of proteins critical to mitochondrial

150   metabolism, including components of the ETC and TCA cycle[19]. Fe-S cluster synthesis is

151   initiated in the mitochondria and requires the coordination of iron and cysteine-derived

152   sulfur by a multi-protein complex (**Figure 3a**). Disrupting this machinery is associated with

153   the loss of ETC function and an increase in ROS production[33,34]. Furthermore,

154   deficiencies in Fe-S cluster synthesis are associated with severe mitochondrial defects

155   underlying varied human pathologies[35]. Considering this, the absence of mitochondrial

156   dysfunction in NSCLC cells under cystine starvation suggests that Fe-S cluster synthesis

157   is sustained.

158

159   To scrutinize this possibility, we evaluated the functionality of mitochondrial Fe-S proteins

160   under cystine deprivation. First, an assessment of the TCA cycle enzyme aconitase

161   (ACO2) in isolated mitochondria showed no change in ACO2 activity upon cystine

162   starvation (**Figure 3b**). Next, we employed a specialized Seahorse-based assay to

163   specifically assess the function of the Fe-S cluster dependent complexes of the ETC[36,37].

164   This revealed that the activities of the respiratory supercomplexes I-III and II-III were not

165   diminished in the absence of extracellular cystine (**Figures 3c and 3d**). Lastly, we

7

166   interrogated the function of the unique Fe-S protein lipoic acid synthetase (LIAS). Rather

167   than simply mediate its catalysis, LIAS' resident Fe-S cluster is consumed during its

168   synthesis of lipoate moieties that facilitate metabolic protein function[38]. We evaluated the

169   lipoylation status of the E2 component of the pyruvate dehydrogenase complex (PDH-

170   E2) and dihydrolipoamide S-succinyltransferase (DLST) as surrogate markers for LIAS

171   activity and found no change in protein lipoylation with respect to cysteine availability

172   (**Figure 3e**). Collectively these data demonstrate a complete maintenance of Fe-S protein

173   function under cystine starvation, suggesting that Fe-S cluster synthesis is sustained

174   despite the absence of cysteine.

175

176   Still, there remained the possibility that Fe-S cluster turnover exceeds the 20h starvation

177   timeframe used for these studies, which would negate the necessity of *de novo* synthesis.

178   To interrogate this, we chelated cellular iron with deferoxamine (DFO) to manipulate the

179   other input of Fe-S cluster synthesis[38]. In contrast to cystine starvation, 20h of iron

180   chelation significantly diminished Fe-S protein function in H1299 cells (**Figures 3f-h**).

181   Importantly, DFO treatment promoted a progressive decrease in respiratory complex

182   function (**Extended Data Figures 2a and 2b**). This suggests that rather than stripping

183   iron from existing clusters and rendering them inactive, iron chelation restricts synthesis

184   of new clusters. Together, these data indicate that NSCLC cells retain the capacity to

185   synthesize Fe-S clusters in the absence of an extracellular cysteine source.

186

187

188

8

189   CHAC1 Supports Fe-S Protein Function Under Cystine Deprivation

190   The maintenance of Fe-S cluster synthesis under cystine starvation argues for the

191   existence of an alternative source of mitochondrial cysteine. Given the absence of

192   mitochondrial oxidative stress and more reduced state of the matrix under cystine

193   starvation (**Figure 2**), we considered the possibility that the antioxidant function of GSH

194   was dispensable, and that the tripeptide could serve as a mitochondrial cysteine sink.

195   Intriguingly, characterization of the transcriptional response to cysteine deprivation has

196   revealed glutathione-specific gamma-glutamylcyclotransferase 1 (CHAC1) as the most

197   highly induced gene[6]. CHAC1 is a component of the intracellular GSH cleavage system

198   (**Figure 4a**), which catabolizes GSH to yield 5-oxoproline and cysteinylglycine (Cys-

199   Gly)[39]. Cys-Gly can then be further cleaved by various peptidases to release its

200   constituent amino acids[40]. Considering this, we hypothesized that CHAC1 induction

201   under cystine starvation would promote cysteine mobilization from GSH to support Fe-S

202   cluster synthesis.

203

204   In our NSCLC cells, we find that cystine starvation elicited a temporal accumulation of

205   CHAC1 protein that coincides with an induction of ATF4 (**Figure 4b**), agreeing with

206   previous reports that CHAC1 is an ATF4 target[39,41]. In contrast, expression of CHAC2,

207   the other intracellular mediator of GSH catabolism was not induced by cystine starvation

208   (**Figure 4b**). Several expansive studies mapping the subcellular distribution of the human

209   proteome have suggested that CHAC1 localizes to multiple organelles, including the

210   mitochondria[42,43]. We generated cells expressing a His-tagged construct within the outer

211   mitochondrial membrane (HA-Mito)[44] to facilitate the purification of mitochondria from cell

212   homogenates and assess CHAC1 expression within the organelle. We found that CHAC1

213   is expressed within the mitochondria of NSCLC cells and that CHAC1 expression within

214   the mitochondria was also increased under cystine starvation (**Figure 4c**). Importantly,

215   CHAC2 does not localize to the mitochondria irrespective of cystine availability,

216   suggesting any effect of GSH catabolism on mitochondrial function is attributable to

217   CHAC1.

218

219   With this confirmation of mitochondrial localization, we next employed the CRISPR/Cas9

220   system[45] to generate CHAC1 knockout cell lines to determine if CHAC1 influences Fe-S

221   protein function by influencing cysteine availability (**Figure 4d**). We found that CHAC1

222   knockout had no detrimental effect on Fe-S protein function in the presence of cystine

223   (**Figures 4e-f**). However, unlike in control cells, the activities of ACO2 and the Fe-S

224   dependent respiratory supercomplexes were diminished to varying degrees under cystine

225   starvation in CHAC1 knockout cells (**Figures 4e-f**). To supplement these findings, we

226   also assessed the influence of CHAC1 expression on Fe-S protein function with a

227   doxycycline-inducible shRNA system (**Extended Data Figure 3a**)[46]. Again, loss of

228   CHAC1 protein did not influence ACO2 or ETC complex activity in the presence of cystine

229   (**Extended Data Figures 3b-d**). Yet, we did observe a significant reduction in the

230   functionality of these Fe-S proteins under cystine deprivation upon CHAC1 knockdown

231   (**Extended Data Figures 3b-d**). To ensure that these effects were specific to CHAC1, we

232   also evaluated the influence of CHAC2 knockdown on Fe-S protein function (**Extended

233   Figure 3e**). Critically, CHAC2 loss had no effect on ACO2 or respiratory chain activity

234   regardless of cystine availability (**Extended Data Figures 3f-h**). Collectively these data

235   indicate that CHAC1 expression is enhanced in the mitochondrial matrix of cystine

236   starved NSCLC cells in a manner that supports the function of Fe-S proteins. Further, this

237   activity is confined to CHAC1 as its homolog CHAC2 is absent from the mitochondria.

238

239   <u>Mitochondrial GSH Supports Fe-S Protein Function in the Absence of Extracellular</u>

240   <u>Cystine</u>

241   To determine if CHAC1 has a discernable influence on the pools of mitochondrial cysteine

242   and GSH in the potential support of Fe-S cluster synthesis, we endeavored to monitor the

243   availability of these metabolites in response to cystine starvation (**Figure 5a**). To

244   accomplish this, we employed an established liquid chromatography-mass spectroscopy

245   (LC-MS) metabolomics scheme that makes use of HA-Mito cells to facilitate the rapid

246   isolation of mitochondria for analysis of matrix metabolite[44,47]. Though this system

247   enables the detection of the wide range of metabolites present within the mitochondria,

248   the nature of this scheme prevents the detection of cysteine due to the high reactivity of

249   its resident thiol[44,48]. To overcome this technical limitation, we utilized the alkylating agent

250   n-ethylmaleimide (NEM)[49] to stabilize thiol containing metabolites. Application of NEM

251   rapidly alkylated cellular thiols, indicated by the stabilization of reduced PRDX3 within 30

252   seconds of treatment (**Extended Data Figure 4a**). Importantly, this did not interfere with

253   the capacity to isolate mitochondria from HA-Mito cells (**Extended Data Figure 4b**).

254

255   We found that this NEM derivatization indeed permitted the detection of mitochondrial

256   cysteine (**Figure 5b and Extended Data Figure 4c**). Consistent with our previous

257   findings[5], cystine starvation promoted the rapid depletion of cellular cysteine (**Figure 5b**

11

258   **and Extended Data Figure 4c**). The rate of exhaustion was similar between the cytosol

259   and matrix, with a half-life of less than 30 minutes across compartments. In contrast,

260   cellular GSH levels declined more gradually over the course of a 20h, with the matrix pool

261   being marginally more stable than the cytosol following starvation (**Figure 5c and**

262   **Extended Data Figure 4d**). We next evaluated the effect of CHAC1 knockdown on

263   cysteine and GSH availability at 12h of cystine starvation. Whereas CHAC1 loss had no

264   discernable effect on matrix cysteine availability, cytosolic cysteine was modestly spared

265   in CHAC1 deficient cells (**Figures 5d and 5e**). We observed a more striking effect on

266   cytosolic GSH levels, which were significantly elevated in the absence of CHAC1 (**Figure**

267   **5f**). This GSH sparing effect was also evident in the matrix, which exhibited similar trends

268   towards increased GSH availability (**Figure 5g**). Together these data indicate that CHAC1

269   is a significant modulator of GSH availability under cystine starvation.

270

271   To interrogate if mitochondrial GSH is a determinant factor of Fe-S protein function under

272   cysteine limitation, we restricted the matrix GSH pool by knocking out the predominant

273   mitochondrial GSH transporter SLC25A39 (**Figure 5h**)[50,51]. We found that like CHAC1,

274   SLC25A39 knockout did not impair Fe-S protein function under cystine replete conditions

275   (**Figures 5i-k**). However, the activities of ACO2 and the Fe-S dependent respiratory

276   complexes were significantly diminished under cystine starvation in the absence of

277   SLC25A39 (**Figures 5i-k**). Collectively these data indicate that CHAC1 catabolism of

278   GSH has a significant influence on GSH availability in response to cystine starvation, and

279   that mitochondrial GSH is critical for Fe-S protein function under these limiting conditions.

280

12

281 <u>Maintenance of Fe-S Clusters is Antagonistic to Survival Under Cystine Starvation</u>

282 To determine if the GSH-dependent maintenance of Fe-S protein function plays a

283 contributing role to ferroptosis in NSCLC we evaluated cell viability under cystine

284 starvation in response to the disruption of Fe-S cluster homeostasis. Beyond synthesis,

285 Fe-S clusters are regulated at the level of their oxidation status (**Figure 6a**)[52,53]. We found

286 that knockdown of components of the core Fe-S cluster biosynthetic complex diminished

287 Fe-S protein function and prolonged survival of H1299 and PC9 cells starved of cystine

288 (**Figure 6b and Extended Data Figures 5a-c**). A previous report found that loss of Fe-S

289 cluster synthesis exacerbated erastin-induced ferroptosis in A549 cells due to an

290 accumulation of iron[54]. Consistent with this report, we find that NFS1 knockdown provides

291 no survival benefit under cystine starvation in A549 cells and that ISCU knockdown

292 exacerbates ferroptosis in these cells (**Extended Data Figures 5a and 5d**). This

293 suggests a cell line dependent response to the targeted disruption of the Fe-S cluster

294 synthesis machinery under cystine starvation. We previously established that the

295 mitochondrial NADPH producing nicotinamide nucleotide transhydrogenase (NNT)

296 supports Fe-S protein function through the mitigation of cluster oxidation[37]. We observed

297 that the decrease in respiratory chain function upon NNT knockdown was associated with

298 an increase in survival under cystine deprivation (**Figure 6c and Extended Data Figures**

299 **5e-g**). Together these data suggest that the maintenance of Fe-S cluster homeostasis is

300 detrimental to cystine starved NSCLC cells.

301

302 We next evaluated if the defect in Fe-S protein function observed with CHAC1 loss under

303 cystine deprivation was also associated with a delay in ferroptosis. Indeed, CHAC1

13

304   knockout significantly prolonged survival under cysteine deprivation (**Figure 6d**). Further,

305   this was associated with a decrease in plasma membrane lipid peroxidation (**Extended**

306   **Data Figure 5h**). To extend this analysis, we determined if CHAC1 knockout influenced

307   the response to other ferroptosis inducers. We found that CHAC1 knockout cells were

308   similarly protected against erastin induction of ferroptosis, but not against the GPX4

309   inhibitor RSL3 (**Figure 6e**). This suggests that the effect of CHAC1 on ferroptosis

310   induction is at least in part due to its effect on the mitochondria, as only cysteine restriction

311   and not GPX4 inhibition-induced ferroptosis has an established mitochondrial

312   component[13]. However, this is unlikely to be a result of CHAC1 sparing of matrix GSH,

313   as SLC25A39 also prolonged survival under cysteine deprivation (**Figure 6f**). Finally, we

314   employed inhibitors of complex I (rotenone) and complex III (myxothiazol) to confirm if the

315   consequence of Fe-S protein function, sustained ETC flux, impacts the induction of

316   ferroptosis. In support of this, we found that both rotenone and myxothiazol prolonged

317   survival in the absence of cystine (**Figure 6g**). In totality, our findings indicate that NSCLC

318   cells sustain their respiratory capacity in response to cysteine deprivation to the detriment

319   of their viability. This is achieved through the maintenance of mitochondrial cysteine

320   metabolism in the form of Fe-S cluster synthesis and depends on the catabolism of

321   mitochondrial GSH by CHAC1 (**Figure 6h**).

322

323   **Discussion**

324

325   Mitochondria are critical mediators of the cellular response to various stressors,

326   integrating both intrinsic and extrinsic signals to modulate their function in support of cell

14

327   resilience[55]. However, there exist instances in which mitochondria compete with the

328   broader cellular milieu to selfishly benefit themselves at the level of the mitochondrial

329   genome[56]. This is likely an ancient relic of endosymbiosis and has a significant impact on

330   human disease[56–58]. Our findings indicate a selfish response to nutrient stress in NSCLC

331   at the level of mitochondrial metabolism. Herein we describe a self-defeating

332   maintenance of respiratory function through the persistence of mitochondrial cysteine

333   metabolism in the absence of an extracellular source. This occurs through an apparent

334   exploitation of the cellular stress response; where the activation of ATF4 in response to

335   cystine starvation drives the expression of CHAC1[39,41].

336

337   CHAC1 is recognized as a potential biomarker for ferroptosis[6,59] and has been implicated

338   in execution of this cell death pathway[59]. However, the mechanism by which CHAC1

339   promotes ferroptosis has not been adequately defined. Our work demonstrates that

340   CHAC1 catabolism of GSH is a significant factor in the depletion of GSH across cellular

341   compartments. In the cytosol of NSCLC cells this is accompanied by an accumulation of

342   ROS[5], which facilitates peroxidation of plasma membrane lipids[8]. Intriguingly, we find that

343   the depletion of matrix GSH is not associated with an accumulation of oxidative stress in

344   NSCLC mitochondria. Instead, the regulated degradation of GSH by CHAC1 actually

345   sustains mitochondrial function through the support of Fe-S cluster synthesis in the

346   absence of a soluble pool. This finding agrees with a recent report uncovering a significant

347   connection between mitochondrial GSH and Fe-S proteins at the organismal level[50], and

348   indicates an aspect of this regulation is at the level of cluster synthesis itself.

349

350   Yet, this persistence of mitochondrial function under cysteine limitation may be a unique

351   characteristic of NSCLC compared to other malignancies. Though mitochondrial

352   metabolism is implicated in ferroptosis, mitochondrial function is reported to progressively

353   decline upon prolonged cysteine deprivation, marked by drastic changes in membrane

354   potential, damage to the IMM, and fragmentation of the mitochondrial network in

355   fibrosarcoma, breast and liver cancers[13,20,59].   Moreover, the systemic depletion of

356   cysteine promoted severe mitochondrial morphological changes and loss of cristae in

357   pancreatic ductal carcinoma[3]. The propensity for lung cancer cells to retain their

358   mitochondrial function under this nutrient stress may be a factor of their tissue of origin.

359   The lung experiences atmospheric oxygen tension upon inspiration, saturating the tissue

360   with this vital nutrient[60]. However, oxygen is incredibly toxic in excess, and the

361   mitochondria serve a critical function in coupling its detoxification to the generation of

362   energy[61]. Alveolar type II cells, which are appreciated as a cell of origin for lung

363   adenocarcinoma[62,63], are enriched with mitochondria to manage the highly oxygenated

364   lung microenvironment[64]. This may contribute to the substantial mitochondrial metabolism

365   exhibited by human lung tumors[23,24] and the necessity for mitochondrial function in lung

366   tumorigenesis[37,65–68]. Considering the importance of mitochondrial function in lung

367   tumors, our data may reflect an inherent prioritization of mitochondrial function in

368   response to stress in NSCLC.

369

370   Prioritization of mitochondrial function causes an apparent misalignment with the capacity

371   to maintain cell viability under cysteine starvation, as our findings reinforce the connection

372   between ETC activity and ferroptosis[13–16]. The connection between this critical aspect of

16

373 mitochondrial metabolism and ferroptosis remains unresolved and is a significant focus

374 of our ongoing work. Though we show that the maintenance of Fe-S protein function by

375 CHAC1 activity in the mitochondria promotes ferroptosis, this does not preclude its effect

376 on cytosolic GSH. We show that CHAC1 loss significantly spares cytosolic GSH under

377 cystine starvation, indicating that GSH catabolism is a relevant factor in the capacity of

378 cells to mitigate lipid peroxidation[10]. Although this is detrimental in the context of cysteine

379 limitation, this explains why CHAC1 expression is restricted under basal conditions[39,41,69].

380 CHAC1 exhibits 20X the catalytic efficiency of CHAC2, which is constitutively expressed

381 for the maintenance of GSH at millimolar levels within the cell[5,70]. Therefore, CHAC1 likely

382 serves a cytoprotective role when excess GSH is detrimental to the cell, such as

383 conditions of reductive stress[71,72]. In light of our findings, a characterization of CHAC1

384 function in response to various redox stressors is highly warranted.

385

386 **Methods**

387

388 <u>Cell Culture</u>

389 Human lung adenocarcinoma cell lines (A549, H322, H1299, H1792, H1975, H2009,

390 PC9) were previously obtained[73] from the Harmon Cancer Center Collection (University

391 of Texas-Southwestern Medical Center) or commercially from the American Type Culture

392 Collection (ATCC) and cultured in RPMI 1640 medium (Fisher Scientific, 11-875-119)

393 supplemented with 5% FBS (Sigma-Aldrich, F0926) in the absence of antibiotics. Cell

394 lines were maintained at 37°C in a humidified incubator containing 95% air and 5% CO_2

395 and routinely tested for mycoplasma contamination with the MycoAlert Assay (Lonza,

17

396   LT07-418). For experiments requiring manipulation of cystine availability, cells were

397   cultured in RPMI 1640 medium without L-glutamine, L-cysteine, L-cystine, and L-

398   methionine (Fisher Scientific, ICN1646454) supplemented with 5% dialyzed FBS (Sigma-

399   Aldrich, F0392), L-glutamine (VWR, VWRL0131-0100), and L-methionine (Sigma-Aldrich,

400   M5308). L-Cystine (Sigma-Aldrich, C6727) was also added back to the deficient media

401   when required. Additional reagents used for the described experiments included: DMSO

402   (VWR, 97063), FCCP (Sigma-Aldrich, C2920), ferrostatin-1 (Cayman Chemical, 17729),

403   Z-VAD-FMK (Fisher Scientific, F7111), cyclosporin A (Fisher Scientific, NC9676992),

404   deferoxamine (DFO; Sigma-Aldrich, D9533), erastin (Cayman Chemical, 17754), RSL3

405   (Cayman Chemical, 19288), rotenone (Sigma-Aldrich, R8875), myxothiazol (Neta

406   Scientific, T5580).

407

408   Viral Infection

409   For the generation of lentivirus, Lenti-X 293T cells (Clontech, 632180) were cultured in

410   DMEM (Fisher Scientific, MT10013CV) supplemented with 5% FBS to 90% confluency.

411   They were then co-transfected in the presence of polyethylenimine (Sigma-Aldrich,

412   408727) with 6μg of the plasmid of interest and 6μg of the packaging plasmids pCMV-

413   VSV-G (Addgene, 8454) and pCMVdR8.2 dvpr (Addgene, 8455) in a 1:8 ratio. Cells were

414   infected in the presence of 8μg/mL polybrene (Santa Cruz Biotechnology, sc-134220A)

415   with lentivirus for 8h at an optimized dilution determined with the Lenti-X GoStix Plus

416   protocol (Takara, 631280). CHAC1 and SLC25A39 knockout cells were generated using

417   the pLenti-CRISPR-V2 plasmid (Addgene, 52961) encoding validated sgRNA sequences

418   towards CHAC1 or SLC25A39[74]. Knockout cells were selected with 1μg/mL puromycin

18

419 (Invivogen, ant-pr-1) for 5d prior to use for experimentation. Additionally, shRNA

420 sequences targeting CHAC1[75] or CHAC2 were cloned into a modified version of the

421 doxycycline inducible LT3GEPIR vector[46], where the puromycin resistance cassette was

422 replaced with a zeocin resistance gene to generate cell lines with temporal control of

423 CHAC1 depletion. These cells were selected in 100μg/mL zeocin (Invivogen, ant-zn-1)

424 for 7d prior to use for experimentation. Finally, shRNA sequences targeting NFS1

425 (Addgene, 102963), ISCU (Addgene, 102972), NNT (Open Biosystems,

426 TRCN0000028507), or a nontargeting control sequence (Scramble; Millipore Sigma,

427 SHC002) in a pLKO.1 vector were used to disrupt the expression of proteins associated

428 with Fe-S cluster homeostasis. Cells were selected in 1μg/mL puromycin for 3d and then

429 used for experimental analysis 4d post-infection.

430

431 For the generation of 3XHA-EGFP-OMP25 (HA-Mito) retrovirus[44], Phoenix-AMPHO 293T

432 cells (ATCC, CRL-3213) were cultured in DMEM supplemented with 5% FBS to 90%

433 confluency. They were then transfected with 6μg of the pMXs-3XHA-EGFP-OMP25

434 (Addgene, 83356) plasmid in the presence of polyethylenimine. Cells were infected in the

435 presence of 8μg/mL polybrene with undiluted retrovirus for 24h, then overlaid with fresh

436 retrovirus for an additional 24h. Retrovirally-infected cells were then selected with

437 10μg/mL blasticidin (Invivogen, ant-bl-1) for 5d prior to use for experimentation.

438

439 Seahorse Analyses of Mitochondrial Function

440 Analyses of mitochondrial metabolic function were performed with a Seahorse XFe96

441 Analyzer (Agilent). General mitochondrial function was assessed based on the Seahorse

19

442   XF Cell Mito Stress Test protocol (Agilent Technologies, Santa Clara, CA, USA). Basal

443   oxygen consumption rate (OCR) was determined by subtracting rotenone and antimycin

444   A (Sigma-Aldrich, A8674) insensitive oxygen consumption from baseline measurements.

445   Coupling efficiency was determined by calculating the proportion of rotenone/antimycin A

446   sensitive oxygen consumption that is also sensitive to oligomycin (Sigma-Aldrich, 75351)

447   treatment. ATP-linked respiration was determined by calculating the fraction of baseline

448   oxygen consumption that is sensitive to ATP synthase inhibition. Finally, maximal

449   respiratory capacity was determined by subtracting the residual oxygen consumption

450   following rotenone/antimycin A treatment from the oxygen consumption stimulated by

451   mitochondrial uncoupling. Fe-S cluster dependent ETC complex function was assessed

452   according to a previously established protocol[36]. Briefly, 40,000 cells were seeded

453   overnight on quadruplicate wells of an XFe96 microplate. Cells were then washed twice

454   with mitochondrial assay solution (220mM mannitol [Sigma-Aldrich, M4125], 70mM

455   sucrose [Sigma-Aldrich, S7903], 10mM KH_2PO_4 [VWR, 470302], 2mM HEPES [Fisher

456   Scientific, BP310], and 1mM EGTA [VWR, 97062]) and then overlaid with 175μL of

457   mitochondrial assay solution supplemented with 10mM sodium pyruvate (Sigma-Aldrich,

458   P5280), 1mM malate (Sigma-Aldrich, M0875), 4mM ADP (Sigma-Aldrich, A5285), and

459   Seahorse Plasma Membrane Permeabilizer (Agilent, 102504-100). Cells were then

460   sequentially subjected to 1μM rotenone to inhibit complex I, 10mM succinate (Sigma-

461   Aldrich, S3674) to stimulate complex II, and finally 1μM antimycin A to inhibit complex III.

462   For assays requiring a period of cystine starvation, 20,000 cells were seeded overnight

463   and then overlaid with cystine replete or deficient RPMI for 20 hours prior to starting the

20

464 assay. Following each assay, cells in each well were lysed to determine protein

465 abundance for normalization.

466

467 Cell Viability

468 Cells were seeded overnight onto black walled 96-well plates at a density of 7,500-12,500

469 cells/well in a total volume of 100μL. The cells were then washed twice with PBS and then

470 overlaid with cystine-free RPMI supplemented with 20nM Sytox Green (Fisher Scientific,

471 S7020) and the indicated treatment. Cells were placed in an IncuCyte S3 live-cell analysis

472 system (Essen BioScience, Ann Arbor MI, USA) or a CellCyte X Live Cell Analyzer

473 (Cytena, Freiburg im Breisgau, Germany) housed in a humidified incubator containing

474 95% air and 5% CO_2 at 37°C. A series of images were acquired every 2-4h with a 10X

475 objective lens in phase contrast and green fluorescence (Ex/Em: 460/524nm with an

476 acquisition time of 200-400ms). Data was processed using IncuCyte S3 2020A (Essen

477 BioScience, Ann Arbor MI, USA) or CellCyte Studio (Cytena, Freiburg im Breisgau,

478 Germany) software. Cell death was calculated as the number of Sytox Green positive

479 cells/mm^2 and normalized to cell confluence (dead cells/mm^2/% confluence). Cell death

480 data were represented as area under the curve (AUC), which represents the sum of dead

481 cells over a 48h period.

482

483 Fluorescence-Based Analyses of ROS

484 Fluorescent probes assessing $\Delta\Psi_m$, mitochondrial density, cellular ROS, mitochondrial

485 $\bullet O_2^-$, H_2O_2, and lipid peroxidation were measured by flow cytometry. For each treatment

486 condition, 10^5 cells were seeded overnight on triplicate wells of a 6-well plate. Cells were

21

487   then washed twice with PBS and overlaid with cystine replete or deficient RPMI for 20

488   hours. $\Delta\Psi_m$ was determined using tetramethylrhodamine (TMRE; Fisher Scientific, T669)

489   as previously described[76]. At 19.5h of treatment, cells were incubated in 250nM TMRE

490   suspended in the appropriate treatment media for 30min at 37°C and then collected for

491   analysis. Mitochondrial density was determined using MitoTracker Green FM

492   (ThermoFisher Scientific, M7514) according to the manufacturer's protocol. Following

493   treatment, cells were incubated in 200nM MitoTracker Green FM in PBS for 15min at

494   37°C and then collected for analysis. Cellular ROS levels were assayed using CellROX

495   Green (ThermoFisher Scientific, C10444) according to the manufacturer's protocol.

496   Briefly, at 19.5h of treatment, 4μL of 2.5mM CellROX Green was applied to each well for

497   a working concentration of 5μM. Cells were incubated at 37°C for the remaining 30min of

498   treatment and then collected for analysis. Mitochondrial $\bullet O_2^-$ was determined with

499   MitoSOX Red (ThermoFisher Scientific, M36008) based on a previously described

500   protocol[77]. Following treatment, cells were incubated in 5μM of MitoSOX Red in PBS for

501   20min at 37°C and then collected for analysis. Mitochondrial H_2O_2 was assessed with

502   MitoPY1 (Fisher Scientific, 442810) according to an established protocol[78]. Following

503   treatment, cells were incubated in 10μM of MitoPY1 in PBS for 20min at 37°C and then

504   collected for analysis. Mitochondrial lipid peroxidation was determined using the

505   ratiometric fluorescent probe MitoPerOX (Cayman Chemical, 18798) according to the

506   manufacturer's protocol. At 19.5h of treatment, cells were incubated in 10μM MitoPerOX

507   suspended in the appropriate treatment media for 30min at 37°C and then collected for

508   analysis. For all analyses, cells were washed twice with ice cold PBS following incubation

509   with the respective probe and collected into 500μL of ice cold PBS for analysis with a BD

22

510   Accuri C6 Plus Flow Cytometer (BD Biosciences, Franklin Lakes, NJ, USA). For TMRE,

511   and MitoSOX Red, a phycoerythrin (PE) optical filter was used for fluorescence detection.

512   For MitoTracker Green, CellROX Green, and MitoPY1, a fluorescein isothiocyanate

513   (FITC) optical filter was used for fluorescence detection. MitoPerOX fluorescence was

514   detected with both the PE and FITC filters to calculate the ratio of oxidized (green) and

515   unaltered (red) membrane lipids. For each analysis, the mean fluorescence intensity of

516   10,000 discrete events was calculated. Whole cell lipid peroxidation was determined

517   using the Image-IT Lipid Peroxidation Kit (ThermoFisher Scientific, C10445) according to

518   the manufacturer's protocol. For each treatment condition, 15,000 cells were seeded

519   overnight onto triplicate wells of a black walled 96-well plate. Cells were then washed with

520   PBS and treated with cystine replete or deficient RPMI for 20h. At 19.5h of treatment, $2\mu L$

521   of 10mM BODIPY-C11 was applied to each well for a working concentration of $10\mu M$.

522   Cells were incubated at $37°C$ for the remaining 30min of treatment. Cells were washed

523   twice with PBS and then placed in a fluorescence-compatible plate reader and

524   fluorescence   measured   (reduced   Ex:475nm/Em:580-640nm,   oxidized

525   Ex:475nm/Em:500-550nm).

526

527   Mitochondrial GSH:GSSG Ratio

528   The oxidation state of the mitochondrial GSH pool was assessed using a previously

529   developed genetically encoded fluorescent and ratiometric biosensor targeted to the

530   mitochondria[32] (Mito-Grx-roGFP2). The Mito-Grx1-roGFP2 construct (Addgene, 64977)

531   was cloned into the pLenti-CMV-Puro vector (Addgene, 17448) and lentivirus generated

532   to produce stable cell lines expressing the biosensor as described. For each treatment

23

533   condition, 15,000 cells were seeded overnight onto triplicate wells of a black walled 96-

534   well plate. Cells were then washed with PBS and treated with cystine replete or deficient

535   RPMI for 16 hours. Cells were then placed in a fluorescence-compatible plate reader

536   (Promega, Madison, WI, USA) and fluorescence measured (GSH-bound

537   Ex:475nm/Em:500-550nm, GSSG-bound Ex:405nm/Em:500-550nm).

538

539   <u>Immunoblotting</u>

540   Following the indicated treatment, cell lysates were generated in ice cold RIPA lysis buffer

541   (20mM Tris-HCl (VWR, 97061-258), pH 7.5, 150mM NaCl (Fisher Scientific, S271), 1mM

542   EGTA, 1mM EDTA [Sigma-Aldrich, E5134], 1% sodium deoxycholate [Sigma-Aldrich,

543   D6750], 1% NP-40 [Sigma-Aldrich, 74385]) supplemented with protease inhibitors (Fisher

544   Scientific, PIA32955). Protein concentrations were then determined by DC Protein Assay

545   (Bio-Rad, 5000112) and 10-30μg samples were prepared with a 6x reducing sample

546   buffer containing β-mercaptoethanol (VWR, M131). Proteins were resolved by SDS-

547   PAGE using NuPAGE 4-12% Bis-Tris precast gels (Fisher Scientfic, WG1402BOX) and

548   then transferred to 0.45μM nitrocellulose membranes (VWR, 10120-006). Membranes

549   were then blocked with 5% nonfat dairy milk in Tris-buffered saline containing 0.1%

550   Tween 20 (VWR, 0777), and incubated overnight with the following primary antibodies:

551   ACC (1:1000; Cell Signaling Technologies, 3662S, RRID:AB_2219400), ATF4 (1:1000;

552   Cell Signaling Technologies, 11815, RRID:AB_2616025), CHAC1 (1:1000; Proteintech,

553   15207-1-AP, RRID:AB_2878118), CHAC2 (1:1000; GeneTex, GTX128819,

554   RRID:AB_2885821), DLST (1:1000; Cell Signaling Technologies, 11954S,

555   RRID:AB_2732907), ERp57 (1:1000; Cell Signaling Technologies, 2881,

24

556   RRID:AB_2160840), HSP60 (1:1000; Cell Signaling Technologies, 4870S,

557   RRID:AB_2295614), HSP90 (1:1000; Cell Signaling Technologies, 4874S,

558   RRID:AB_2121214), ISCU (1:1000; Santa Cruz Biotechnology, sc-373694,

559   RRID:AB_10918261), Lipoic Acid (1:1000; Millipore Sigma, 437695-100UL,

560   RRID:AB_10683357), MCU (1:1000; Cell Signaling Technologies, 14997S,

561   RRID:AB_2721812), NFS1 (1:1000; Santa Cruz Biotechnology, sc-365308,

562   RRID:AB_10843245), NNT (1:1000; Abcam, ab110352, RRID:AB_10887748), PDH-E2

563   (1:1000; Abcam, ab126224, RRID:AB_11129511), PRDX3 (1:1000; Abcam, ab73349,

564   RRID:AB_1860862), SHMT2 (1:1000; Cell Signaling Technologies, 12762S,

565   RRID:AB_2798018), SLC25A39 (1:1000; Proteintech, 14963-1-AP, RRID:AB_2878095),

566   TOM20 (1:1000; Santa Cruz Biotechnology, sc-17764, RRID:AB_628381), α-Tubulin

567   (1:1000; Abcam, ab7291, RRID:AB_2241126). HRP-conjugated anti-mouse (1:10,000;

568   Jackson ImmunoResearch, 115-005-003, RRID:AB_2338447) and anti-rabbit (1:10,000;

569   Jackson ImmunoResearch, 111-005-003, RRID:AB_2337913) secondary antibodies and

570   enhanced chemiluminescence were then used for all immunoblotting.

571

572   For the determination of the PRDX3 oxidation state, a previously established redox

573   immunoblotting protocol was employed[79]. Briefly, following the indicated treatment, cells

574   were washed twice with PBS and overlaid with 200 μL of alkylation buffer (40 mM HEPES,

575   50 mM NaCl, 1 mM EGTA, protease inhibitors) supplemented with 25 mM N-

576   ethylmaleimide (NEM; Fisher Scientific, AA4052606). Cells were incubated for 10 minutes

577   at room temperature and then 20 μL of 10% CHAPS detergent (Sigma-Aldrich, C3023)

578   was added and cells incubated at room temperature for an additional 10 minutes to lyse

25

579   cells. Lysates were then cleared by centrifugation at 4 °C for 15 minutes at 17,000 g.

580   Supernatants were isolated to quantify protein and 5-10 μg protein samples were mixed

581   with a 4X non-reducing buffer prior to separation by SDS-PAGE as described.

582

583   ACO2 Activity

584   Mitochondrial aconitase (ACO2) activity was determined as we have previously

585   described[37]. Briefly, cystine fed or starved cells were collected and resuspended in 200μL

586   of 50mM Tris-HCl and 150mM NaCl, pH 7.4. Cells were then homogenized by dounce

587   homogenizer (15 strokes) and the homogenate spun down at 4°C for 10min at 10,000 g.

588   Organellar pellet was then washed twice and resuspended in 100μL of 1% Triton X-100

589   (VWR, 0694) in 50mM Tris-HCl and 150mM NaCl, pH 7.4 to lyse the mitochondrial

590   membrane. Lysates were then spun down at 4°C for 15 minutes at 17,000 g. Protein

591   concentrations were then determined by DC Protein Assay, and 175μL of 100-500 μg/mL

592   protein were generated in 50mM Tris-HCl, pH 7.4 and incubated at 37°C for 15 minutes.

593   50μL of this protein solution was transferred to triplicate wells of a black walled 96-well

594   plate containing 50μL of 50mM Tris-HCl, pH 7.4. Next, 50μL of a 4mM NADP$^+$ (Neta

595   Scientific, SPCM-N1131-OM) and 20 U/mL IDH1 (Sigma-Aldrich, I1877) solution and

596   50μL of 10mM sodium citrate were sequentially added to initiate the assay. The plate was

597   transferred to a fluorescence-compatible plate reader maintained at 37°C to measure the

598   change in NADPH autofluorescence every minute over a period of 45 minutes. The

599   accumulation of NADPH autofluorescence over time is an indicator of aconitase activity,

600   where ACO2 present in the sample converts the supplied citrate to isocitrate, which is

601   subsequently metabolized by the supplied IDH1 in a reaction that yields NADPH.

26

602

603   <u>Mitochondrial Immunoprecipitation</u>

604   An established protocol for the rapid isolation of mitochondria from HA-Mito cells[44] was

605   modified as follows to preserve thiol containing metabolites and permit their detection by

606   LC-MS. Prior to mitochondrial isolation, 50-200μL of Pierce Anti-HA magnetic beads

607   (VWR, PI88837) were washed in KPBS (136mM KCl [Sigma-Aldrich, P5405], 10mM

608   KH_2PO_4, pH 7.4 in HPLC grade H_2O [Fisher Chemical, W5-1]) for each sample. Samples

609   were processed one at a time in a 4°C cold room to best preserve the metabolic state of

610   each sample. Cells were washed twice with ice cold KPBS and then incubated in KPBS

611   supplemented with 25mM NEM and 10mM ammonium formate (Fisher Scientific,

612   501454965) for 1min. Cells were then washed twice more and collected into ice cold

613   KPBS. Cells were pelleted at 1,000 g for 2min and then resuspended in 200μL of KPBS.

614   Cells were homogenized by Dounce homogenizer (25 strokes), and the homogenate

615   spun down at 1,000 g for 2min. The supernatant was then applied to the pre-washed

616   magnetic beads and incubated on an end-over-end rotator for 3.5min. Beads were then

617   isolated from solution with a DynaMag-2 magnetic stand (ThermoFisher Scientific,

618   12321D). The unbound solution was kept as a mitochondrial-free cytosolic fraction.

619   Mitochondria-bound beads were washed twice with KPBS and then processed for either

620   immunoblotting or metabolite detection. For the purposes of immunoblotting, isolated

621   beads were reconstituted in 50μL of lysis buffer (50mM Tris-HCl, pH 7.4, 150mM NaCl,

622   1mM EDTA, 1% Triton X-100, protease inhibitors), incubated on ice for 10min and lysates

623   cleared by centrifugation at 17,000 g for 10 minutes. Protein was quantified and samples

624   prepared for SDS-PAGE. For metabolite detection, beads were reconstituted in 50μL of

27

625   80% methanol containing 20 μM of [$^{13}C_3$, ^{15}N]-NEM-Cysteine (Cambridge Isotope

626   Laboratories, CNLM-38710H-0.25) and 40 μM of [$^{13}C_2$, ^{15}N]-NEM-GSH (Sigma-Aldrich,

627   683620), incubated on ice for 5 minutes, and extracts cleared by centrifugation at 17,000

628   *g* for 10 minutes. NEM-derivatized standards were prepared as previously described[5].

629   Alternatively, the mitochondrial-free cytosolic fractions were extracted in 800μL of the

630   defined extraction solution, incubated on ice for 5 minutes, and cleared by centrifugation

631   at 17,000 *g* for 10 minutes.

632

633   <u>LC-MS-Based Metabolite Detection</u>

634   For determination of the relative Cys and GSH pool sizes across compartments,

635   previously established LC-MS conditions were employed[5,22] For chromatographic

636   metabolite separation, a Vanquish UPLC system was coupled to a Q Exactive HF (QE-

637   HF) mass spectrometer equipped with HESI (Thermo Fisher Scientific, Waltham, MA,

638   USA). Samples were run on an Atlantis Premier BEH Z-HILIC VanGuard FIT column,

639   2.5μm, 2.1mm x 150mm (Waters, Milford, MA, USA). The mobile phase A was 10mM

640    $(NH_4)_2CO_3$ and 0.05% NH_4OH in H_2O, while mobile phase B was 100% ACN. The column

641   chamber temperature was set to 30°C. The mobile phase condition was set according to

642   the following gradient: 0-13min: 80% to 20% of mobile phase B, 13-15min: 20% of mobile

643   phase B. The ESI ionization mode was negative, and the MS scan range (m/z) was set

644   to 65-975. The mass resolution was 120,000 and the AGC target was 3 x 10^6. The

645   capillary voltage and capillary temperature were set to 3.5 kV and 320°C, respectively.

646   5μL of sample was loaded. The LC-MS metabolite peaks were manually identified and

28

647 integrated by El-Maven (Version 0.3.1) by matching with a previously established in-

648 house library[5].

649

650 <u>Statistical Analysis</u>

651 All data were analyzed for statistical significance with GraphPad Prism 9.4.1 software; P

652 values <0.05 were deemed significant (n.s., not significant, *, P<0.05, **, P<0.01, ***,

653 P<0.001, ****, P<0.0001). Comparisons of two groups were performed with a two-tailed

654 unpaired Student's *t*-test. For comparisons of a single variable in 3 or more groups a one-

655 way ANOVA with a Dunnet's multiple comparisons test was performed. For comparisons

656 of two variables a two-way ANOVA with a Sidak's multiple comparisons test was

657 performed.

658

659 **Data Availability**

660

661 All data supporting the findings of this study are available from the corresponding authors

662 on request.

663

664 **Acknowledgements**

665

673

Contributions

675

676   N.P.W. conceived the study, designed and performed the experiments, analyzed the

677   data, and wrote the manuscript; S.J.Y. performed LC-MS analysis of thiol metabolites;

678   T.F. generated CHAC1-knockout lines and performed immunoblotting; A.S. generated

679   SLC25A39-knockout lines and performed immunoblotting, J.M. characterized CHAC1

680   localization and expression in response to Cys_2 starvation; G.M.D. conceived the study,

681   acquired funding, contributed to the experimental design, supervised the project, and

682   wrote the manuscript.

683

Ethics declarations

685

<u>Competing interests</u>

687

688   The authors declare no competing interests.

689
690
References
692
693   1. Ward, N. P. & DeNicola, G. M. Sulfur metabolism and its contribution to malignancy. *Int. Rev.*
694   *Cell Mol. Biol.* **347**, 39–103 (2019).
695   2. Cramer, S. L. *et al.* Systemic depletion of L-cyst(e)ine with cyst(e)inase increases reactive
696   oxygen species and suppresses tumor growth. *Nat. Med.* **23**, 120–127 (2017).

30

697   3. Badgley, M. A. *et al.* Cysteine depletion induces pancreatic tumor ferroptosis in mice. *Science*
698   **368**, 85–89 (2020).

699   4. Lei, G., Zhuang, L. & Gan, B. Targeting ferroptosis as a vulnerability in cancer. *Nat. Rev.*
700   *Cancer* **22**, 381–396 (2022).

701   5. Kang, Y. P. *et al.* Non-canonical Glutamate-Cysteine Ligase Activity Protects against
702   Ferroptosis. *Cell Metab.* **33**, 174-189.e7 (2021).

703   6. Dixon, S. J. *et al.* Pharmacological inhibition of cystine-glutamate exchange induces
704   endoplasmic reticulum stress and ferroptosis. *eLife* **3**, e02523 (2014).

705   7. Dixon, S. J. *et al.* Ferroptosis: an iron-dependent form of nonapoptotic cell death. *Cell* **149**,
706   1060–1072 (2012).

707   8. Jiang, X., Stockwell, B. R. & Conrad, M. Ferroptosis: mechanisms, biology and role in disease.
708   *Nat. Rev. Mol. Cell Biol.* **22**, 266–282 (2021).

709   9. Doll, S. *et al.* FSP1 is a glutathione-independent ferroptosis suppressor. *Nature* **575**, 693–698
710   (2019).

711   10.   Ingold, I. *et al.* Selenium Utilization by GPX4 Is Required to Prevent Hydroperoxide-
712   Induced Ferroptosis. *Cell* **172**, 409-422.e21 (2018).

713   11.   Magtanong, L. *et al.* Context-dependent regulation of ferroptosis sensitivity. *Cell Chem.*
714   *Biol.* **29**, 1409-1418.e6 (2022).

715   12.   Gao, M., Monian, P., Quadri, N., Ramasamy, R. & Jiang, X. Glutaminolysis and Transferrin
716   Regulate Ferroptosis. *Mol. Cell* **59**, 298–308 (2015).

717   13.   Gao, M. *et al.* Role of Mitochondria in Ferroptosis. *Mol. Cell* **73**, 354-363.e3 (2019).

718   14.   Lee, H. *et al.* Energy-stress-mediated AMPK activation inhibits ferroptosis. *Nat. Cell Biol.*
719   **22**, 225–234 (2020).

720   15.   Gan, B. Mitochondrial regulation of ferroptosis. *J. Cell Biol.* **220**, e202105043 (2021).

721   16.   Homma, T., Kobayashi, S., Sato, H. & Fujii, J. Superoxide produced by mitochondrial
722   complex III plays a pivotal role in the execution of ferroptosis induced by cysteine starvation.
723   *Arch. Biochem. Biophys.* **700**, 108775 (2021).

724   17.   Sun, Y., Zheng, Y., Wang, C. & Liu, Y. Glutathione depletion induces ferroptosis,
725   autophagy, and premature cell senescence in retinal pigment epithelial cells. *Cell Death Dis.*
726   **9**, 753 (2018).

727   18.   Akaike, T. *et al.* Cysteinyl-tRNA synthetase governs cysteine polysulfidation and
728   mitochondrial bioenergetics. *Nat. Commun.* **8**, 1177 (2017).

729   19.   Maio, N. & Rouault, T. A. Outlining the Complex Pathway of Mammalian Fe-S Cluster
730   Biogenesis. *Trends Biochem. Sci.* **45**, 411–426 (2020).

731   20.   Yuan, H., Li, X., Zhang, X., Kang, R. & Tang, D. CISD1 inhibits ferroptosis by protection
732   against mitochondrial lipid peroxidation. *Biochem. Biophys. Res. Commun.* **478**, 838–844
733   (2016).

734   21.   Neitemeier, S. *et al.* BID links ferroptosis to mitochondrial cell death pathways. *Redox*
735   *Biol.* **12**, 558–570 (2017).

736   22.   Kang, Y. P. *et al.* Cysteine dioxygenase 1 is a metabolic liability for non-small cell lung
737   cancer. *eLife* **8**, (2019).

738   23.   Hensley, C. T. *et al.* Metabolic Heterogeneity in Human Lung Tumors. *Cell* **164**, 681–694
739   (2016).

740   24.   Faubert, B. *et al.* Lactate Metabolism in Human Lung Tumors. *Cell* **171**, 358-371.e9
741   (2017).
742   25.   Yagoda, N. *et al.* RAS-RAF-MEK-dependent oxidative cell death involving voltage-
743   dependent anion channels. *Nature* **447**, 864–868 (2007).
744   26.   DeHart, D. N. *et al.* Opening of voltage dependent anion channels promotes reactive
745   oxygen species generation, mitochondrial dysfunction and cell death in cancer cells.
746   *Biochem. Pharmacol.* **148**, 155–162 (2018).
747   27.   Poursaitidis, I. *et al.* Oncogene-Selective Sensitivity to Synchronous Cell Death following
748   Modulation of the Amino Acid Nutrient Cystine. *Cell Rep.* **18**, 2547–2556 (2017).
749   28.   Prola, A. *et al.* Cardiolipin content controls mitochondrial coupling and energetic
750   efficiency in muscle. *Sci. Adv.* **7**, eabd6322 (2021).
751   29.   Murphy, M. P. How mitochondria produce reactive oxygen species. *Biochem. J.* **417**, 1–
752   13 (2009).
753   30.   Harris, I. S. *et al.* Glutathione and thioredoxin antioxidant pathways synergize to drive
754   cancer initiation and progression. *Cancer Cell* **27**, 211–222 (2015).
755   31.   Aon, M. A. *et al.* Glutathione/thioredoxin systems modulate mitochondrial H2O2
756   emission: an experimental-computational study. *J. Gen. Physiol.* **139**, 479–491 (2012).
757   32.   Gutscher, M. *et al.* Real-time imaging of the intracellular glutathione redox potential.
758   *Nat. Methods* **5**, 553–559 (2008).
759   33.   Gomez, M. *et al.* Malfunctioning of the iron-sulfur cluster assembly machinery in
760   Saccharomyces cerevisiae produces oxidative stress via an iron-dependent mechanism,
761   causing dysfunction in respiratory complexes. *PloS One* **9**, e111585 (2014).
762   34.   Wang, J. *et al.* ISCA2 deficiency leads to heme synthesis defects and impaired erythroid
763   differentiation in K562 cells by indirect ROS-mediated IRP1 activation. *Biochim. Biophys. Acta*
764   *Mol. Cell Res.* **1869**, 119307 (2022).
765   35.   Rouault, T. A. & Tong, W. H. Iron-sulfur cluster biogenesis and human disease. *Trends*
766   *Genet. TIG* **24**, 398–407 (2008).
767   36.   Salabei, J. K., Gibb, A. A. & Hill, B. G. Comprehensive measurement of respiratory activity
768   in permeabilized cells using extracellular flux analysis. *Nat. Protoc.* **9**, 421–438 (2014).
769   37.   Ward, N. P., Kang, Y. P., Falzone, A., Boyle, T. A. & DeNicola, G. M. Nicotinamide
770   nucleotide transhydrogenase regulates mitochondrial metabolism in NSCLC through
771   maintenance of Fe-S protein function. *J. Exp. Med.* **217**, (2020).
772   38.   Crooks, D. R. *et al.* Acute loss of iron-sulfur clusters results in metabolic reprogramming
773   and generation of lipid droplets in mammalian cells. *J. Biol. Chem.* **293**, 8297–8311 (2018).
774   39.   Crawford, R. R. *et al.* Human CHAC1 Protein Degrades Glutathione, and mRNA Induction
775   Is Regulated by the Transcription Factors ATF4 and ATF3 and a Bipartite ATF/CRE Regulatory
776   Element. *J. Biol. Chem.* **290**, 15878–15891 (2015).
777   40.   Calabrese, G., Morgan, B. & Riemer, J. Mitochondrial Glutathione: Regulation and
778   Functions. *Antioxid. Redox Signal.* **27**, 1162–1177 (2017).
779   41.   Mungrue, I. N., Pagnon, J., Kohannim, O., Gargalovic, P. S. & Lusis, A. J. CHAC1/MGC4504
780   is a novel proapoptotic component of the unfolded protein response, downstream of the
781   ATF4-ATF3-CHOP cascade. *J. Immunol. Baltim. Md 1950* **182**, 466–476 (2009).
782   42.   Uhlén, M. *et al.* Proteomics. Tissue-based map of the human proteome. *Science* **347**,
783   1260419 (2015).

784   43.   Thul, P. J. *et al.* A subcellular map of the human proteome. *Science* **356**, eaal3321
785   (2017).
786   44.   Chen, W. W., Freinkman, E. & Sabatini, D. M. Rapid immunopurification of mitochondria
787   for metabolite profiling and absolute quantification of matrix metabolites. *Nat. Protoc.* **12**,
788   2215–2231 (2017).
789   45.   Hsu, P. D., Lander, E. S. & Zhang, F. Development and applications of CRISPR-Cas9 for
790   genome engineering. *Cell* **157**, 1262–1278 (2014).
791   46.   Fellmann, C. *et al.* An optimized microRNA backbone for effective single-copy RNAi. *Cell*
792   *Rep.* **5**, 1704–1713 (2013).
793   47.   Bayraktar, E. C. *et al.* MITO-Tag Mice enable rapid isolation and multimodal profiling of
794   mitochondria from specific cell types in vivo. *Proc. Natl. Acad. Sci. U. S. A.* **116**, 303–312
795   (2019).
796   48.   Bak, D. W., Bechtel, T. J., Falco, J. A. & Weerapana, E. Cysteine reactivity across the
797   subcellular universe. *Curr. Opin. Chem. Biol.* **48**, 96–105 (2019).
798   49.   Cox, A. G., Winterbourn, C. C. & Hampton, M. B. Measuring the redox state of cellular
799   peroxiredoxins by immunoblotting. *Methods Enzymol.* **474**, 51–66 (2010).
800   50.   Wang, Y. *et al.* SLC25A39 is necessary for mitochondrial glutathione import in
801   mammalian cells. *Nature* **599**, 136–140 (2021).
802   51.   Shi, X. *et al.* Combinatorial GxGxE CRISPR screen identifies SLC25A39 in mitochondrial
803   glutathione transport linking iron homeostasis to OXPHOS. *Nat. Commun.* **13**, 2483 (2022).
804   52.   Boyd, E. S., Thomas, K. M., Dai, Y., Boyd, J. M. & Outten, F. W. Interplay between oxygen
805   and Fe-S cluster biogenesis: insights from the Suf pathway. *Biochemistry* **53**, 5834–5847
806   (2014).
807   53.   Crack, J. C., Green, J., Thomson, A. J. & Le Brun, N. E. Iron-sulfur clusters as biological
808   sensors: the chemistry of reactions with molecular oxygen and nitric oxide. *Acc. Chem. Res.*
809   **47**, 3196–3205 (2014).
810   54.   Alvarez, S. W. *et al.* NFS1 undergoes positive selection in lung tumours and protects cells
811   from ferroptosis. *Nature* **551**, 639–643 (2017).
812   55.   Manoli, I. *et al.* Mitochondria as key components of the stress response. *Trends*
813   *Endocrinol. Metab. TEM* **18**, 190–198 (2007).
814   56.   Gitschlag, B. L. *et al.* Homeostatic Responses Regulate Selfish Mitochondrial Genome
815   Dynamics in C. elegans. *Cell Metab.* **24**, 91–103 (2016).
816   57.   O'Malley, M. A. Endosymbiosis and its implications for evolutionary theory. *Proc. Natl.*
817   *Acad. Sci. U. S. A.* **112**, 10270–10277 (2015).
818   58.   Dubie, J. J., Caraway, A. R., Stout, M. M., Katju, V. & Bergthorsson, U. The conflict within:
819   origin, proliferation and persistence of a spontaneously arising selfish mitochondrial
820   genome. *Philos. Trans. R. Soc. Lond. B. Biol. Sci.* **375**, 20190174 (2020).
821   59.   Chen, M.-S. *et al.* CHAC1 degradation of glutathione enhances cystine-starvation-
822   induced necroptosis and ferroptosis in human triple negative breast cancer cells via the
823   GCN2-eIF2α-ATF4 pathway. *Oncotarget* **8**, 114588–114602 (2017).
824   60.   Ortiz-Prado, E., Dunn, J. F., Vasconez, J., Castillo, D. & Viscor, G. Partial pressure of
825   oxygen in the human body: a general review. *Am. J. Blood Res.* **9**, 1–14 (2019).
826   61.   Sung, H. J. *et al.* Mitochondrial respiration protects against oxygen-associated DNA
827   damage. *Nat. Commun.* **1**, 5 (2010).

33

828 62. Xu, X. *et al.* Evidence for type II cells as cells of origin of K-Ras-induced distal lung
829 adenocarcinoma. *Proc. Natl. Acad. Sci. U. S. A.* **109**, 4910–4915 (2012).
830 63. Lin, C. *et al.* Alveolar type II cells possess the capability of initiating lung tumor
831 development. *PloS One* **7**, e53817 (2012).
832 64. Schumacker, P. T. *et al.* Mitochondria in lung biology and pathology: more than just a
833 powerhouse. *Am. J. Physiol. Lung Cell. Mol. Physiol.* **306**, L962-974 (2014).
834 65. Davidson, S. M. *et al.* Environment Impacts the Metabolic Dependencies of Ras-Driven
835 Non-Small Cell Lung Cancer. *Cell Metab.* **23**, 517–528 (2016).
836 66. Padanad, M. S. *et al.* Fatty Acid Oxidation Mediated by Acyl-CoA Synthetase Long Chain
837 3 Is Required for Mutant KRAS Lung Tumorigenesis. *Cell Rep.* **16**, 1614–1628 (2016).
838 67. Mayers, J. R. *et al.* Tissue of origin dictates branched-chain amino acid metabolism in
839 mutant Kras-driven cancers. *Science* **353**, 1161–1165 (2016).
840 68. Rao, S. *et al.* AIF-regulated oxidative phosphorylation supports lung cancer
841 development. *Cell Res.* **29**, 579–591 (2019).
842 69. Nguyen, Y. T. K. *et al.* Structural and Functional Analyses of Human ChaC2 in Glutathione
843 Metabolism. *Biomolecules* **10**, E31 (2019).
844 70. Kaur, A. *et al.* ChaC2, an Enzyme for Slow Turnover of Cytosolic Glutathione. *J. Biol.
845 Chem.* **292**, 638–651 (2017).
846 71. Zhang, H. *et al.* Glutathione-dependent reductive stress triggers mitochondrial oxidation
847 and cytotoxicity. *FASEB J. Off. Publ. Fed. Am. Soc. Exp. Biol.* **26**, 1442–1451 (2012).
848 72. Peris, E. *et al.* Antioxidant treatment induces reductive stress associated with
849 mitochondrial dysfunction in adipocytes. *J. Biol. Chem.* **294**, 2340–2352 (2019).
850 73. DeNicola, G. M. *et al.* NRF2 regulates serine biosynthesis in non-small cell lung cancer.
851 *Nat. Genet.* **47**, 1475–1481 (2015).
852 74. Birsoy, K. *et al.* An Essential Role of the Mitochondrial Electron Transport Chain in Cell
853 Proliferation Is to Enable Aspartate Synthesis. *Cell* **162**, 540–551 (2015).
854 75. Yang, X. *et al.* A public genome-scale lentiviral expression library of human ORFs. *Nat.
855 Methods* **8**, 659–661 (2011).
856 76. Ward, N. P., Poff, A. M., Koutnik, A. P. & D'Agostino, D. P. Complex I inhibition augments
857 dichloroacetate cytotoxicity through enhancing oxidative stress in VM-M3 glioblastoma cells.
858 *PloS One* **12**, e0180061 (2017).
859 77. Kauffman, M. E. *et al.* MitoSOX-Based Flow Cytometry for Detecting Mitochondrial ROS.
860 *React. Oxyg. Species Apex NC* **2**, 361–370 (2016).
861 78. Dickinson, B. C., Lin, V. S. & Chang, C. J. Preparation and use of MitoPY1 for imaging
862 hydrogen peroxide in mitochondria of live cells. *Nat. Protoc.* **8**, 1249–1259 (2013).
863 79. Cox, A. G. *et al.* Mitochondrial peroxiredoxin 3 is more resilient to hyperoxidation than
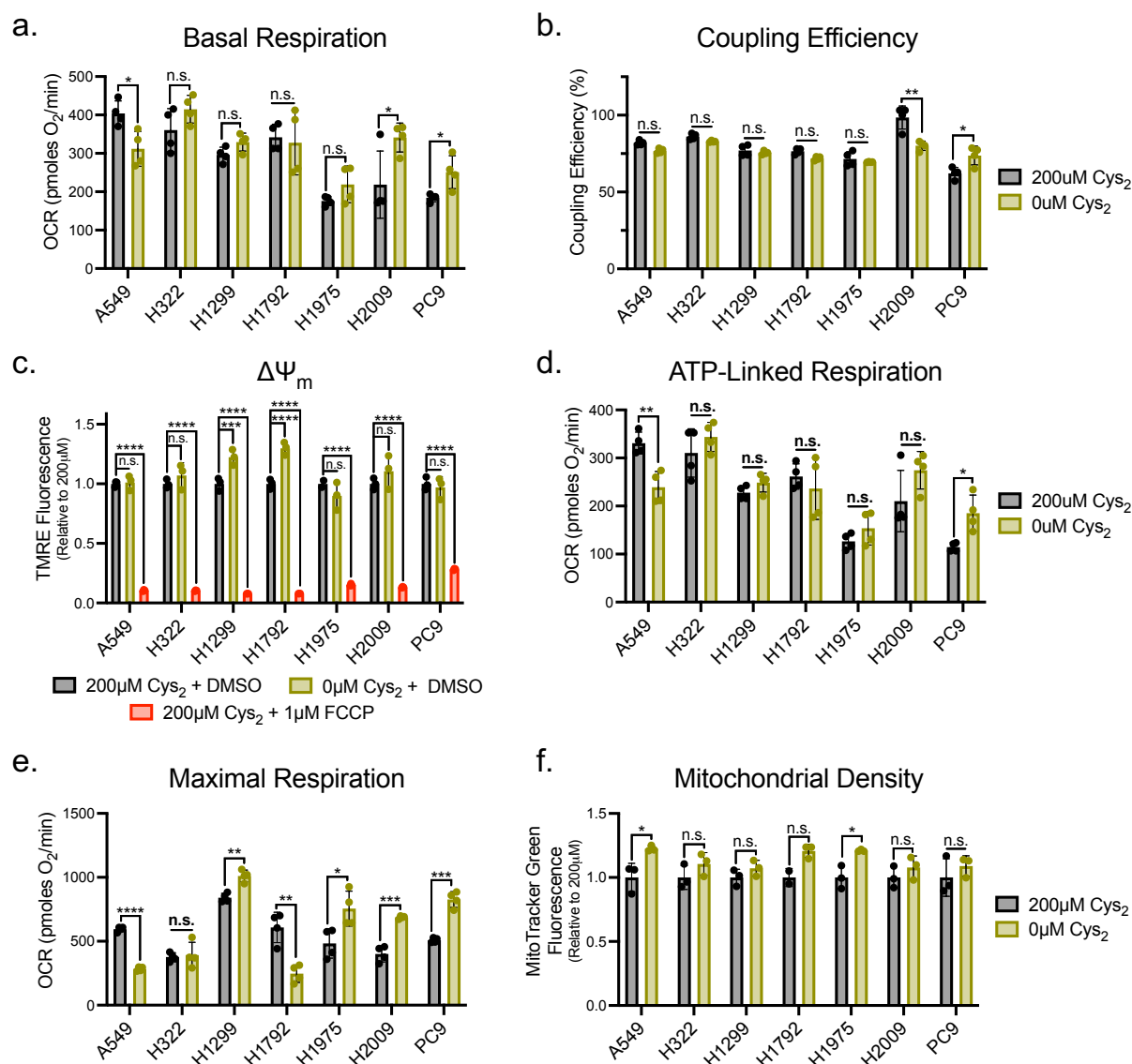864 cytoplasmic peroxiredoxins. *Biochem. J.* **421**, 51–58 (2009).
865

866

867

Figure 1: Mitochondrial Respiration is Sustained in the Absence of Extracellular Cys$_2$. a, Basal oxygen consumption rate of NSCLC cells stimulated with 10mM glucose and 2mM L-glutamine following culture in the presence or absence of cystine (n=4 per condition). **b**, Percentage of basal oxygen consumption linked to the generation of ATP in NSCLC cells fed or starved of cystine (n=4 per condition). **c**, Average relative TMRE fluorescence of NSCLC cells cultured with indicated [cystine] or treated with FCCP for 15 minutes (n=3 per condition). **d**, Oligomycin-sensitive oxygen consumption rate of cystine-

875   fed or starved NSCLC cells (n=4 per condition). **e**, FCCP-stimulated oxygen consumption

876   rate in in NSCLC cells fed or starved of cystine (n=4 per condition). **f**, Average relative

877   MitoTracker Green fluorescence of NSCLC cells cultured in the presence or absence of

878   cystine (n=3 per condition). For all experiments, cells were cultured in the indicated

879   [cystine] for 20 hours prior to the indicated analysis. Data represent mean values ± s.d;

880   n.s., not significant, *, P<0.05, **, P<0.01, ***, P<0.001, ****, P<0.0001. For **a**, **b**, **d-f**, P

881   values were calculated using unpaired Student's *t*-test. For **c**, P values were calculated

882   using a one-way ANOVA. All data are representative of at least 3 experimental replicates.

883
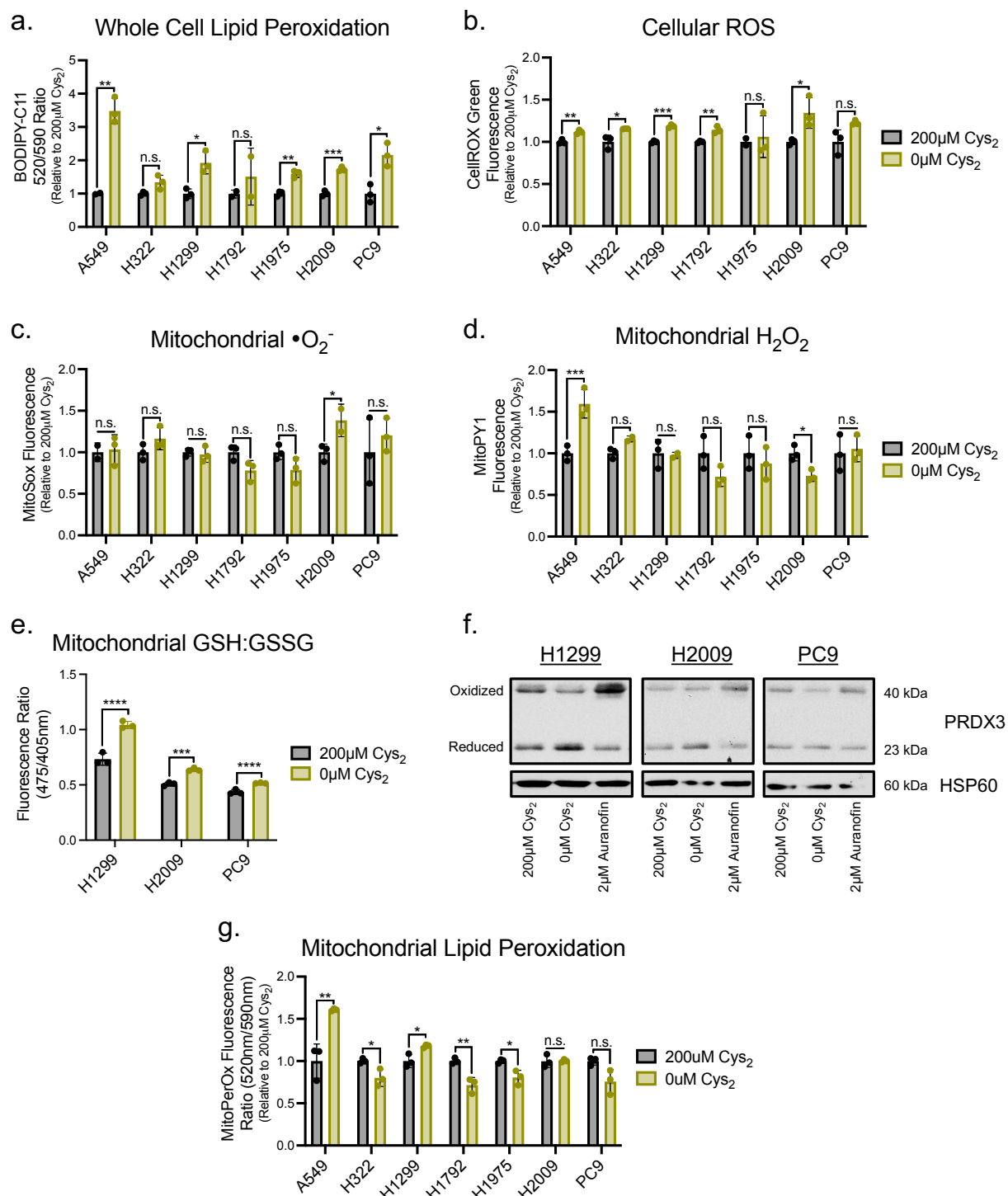
Figure 2: **Cys$_2$ Starvation Does Not Promote Mitochondrial Oxidative Stress**. **a-d**,

Following culture in the presence or absence of cystine, NSCLC cells were treated with

ROS-sensitive fluorescent dyes to determine the average relative levels of **a**, cellular

887   membrane lipid peroxides, **b**, cellular ROS, **c**, mitochondrial superoxide, or **d**,

888   mitochondrial hydrogen peroxide (n=3 per condition for each experiment). **e**, Ratio of

889   Mito-Grx1-roGFP2 fluorescence as indicative of the proportion of the biosensor bound to

890   reduced (GSH) or oxidized (GSSG) glutathione in H1299, H2009, and PC9 cells cultured

891   with or without cystine for 16 hours (n=3 per condition). **f**, Redox immunoblotting of

892   HSP60 and the PRDX3 oxidation state in H1299, H2009, and PC9 cells following culture

893   with the indicated [cystine] or 1 hour treatment with auranofin. **g**, Relative MitoPerOX

894   fluorescence ratio of NSCLC cells cultured in the presence or absence of cystine to

895   indicate the extent of mitochondrial membrane lipid peroxidation (n=3 per condition). For

896   **a-d**, **f**, and **g** cells were cultured in the indicated [cystine] for 20 hours prior to the indicated

897   analysis. Data represent mean values ± s.d; n.s., not significant, *, P<0.05, **, P<0.01,

898   ***, P<0.001, ****, P<0.0001. For **a-e**, and **g**, P values were calculated using two-tailed

899   unpaired Student's *t*-test. All data are representative of at least 3 experimental replicates.
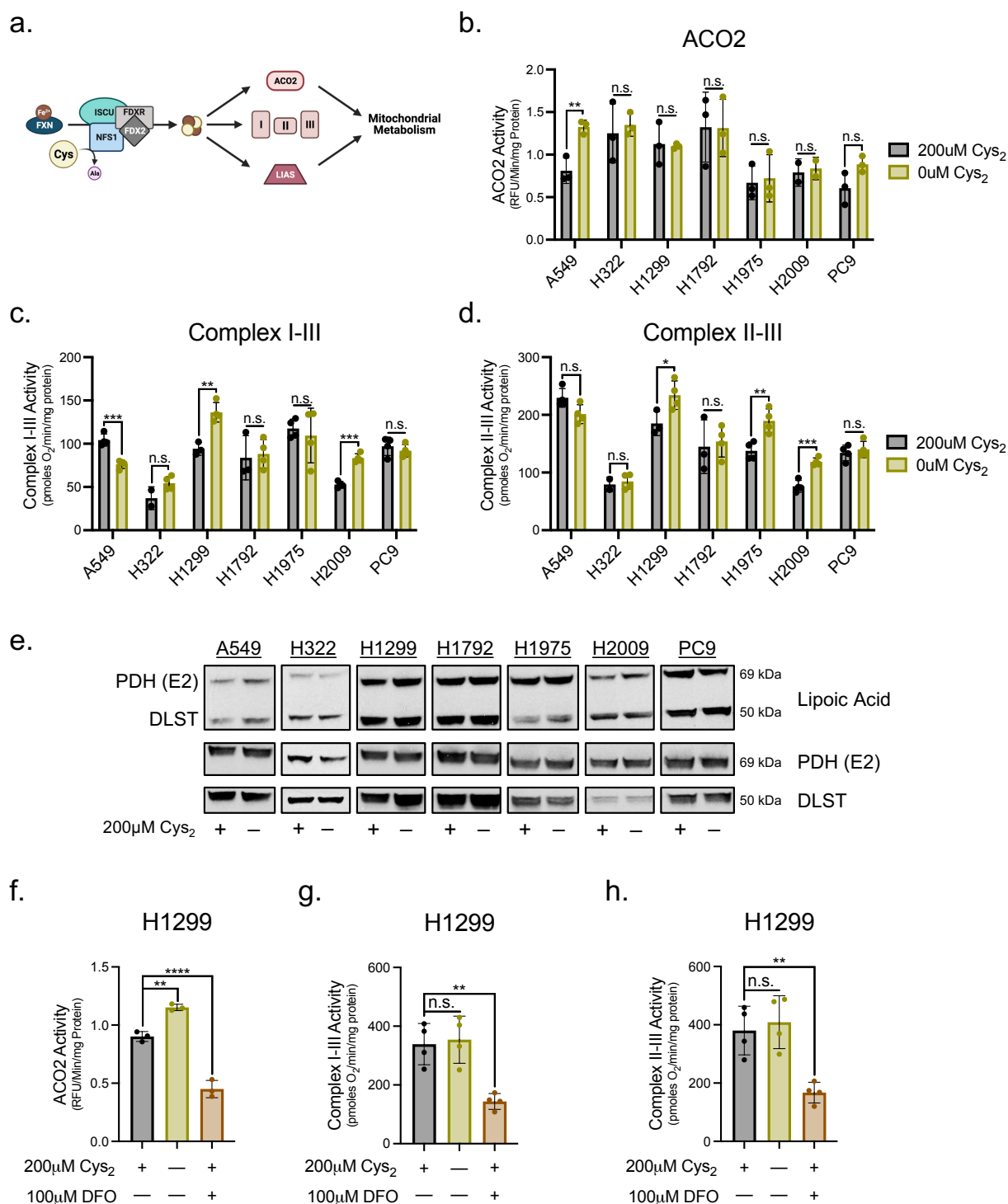
Figure 3: **Fe-S Protein Function is Preserved Under Cys$_2$ Deprivation**. **a**, Schematic of Fe-S cluster synthesis and its contribution to enzymatic function that supports mitochondrial metabolism. **b**, ACO2 activity in mitochondrial lysates of NSCLC cells fed

904   or starved of cystine (n=3 per condition). **c**, Supercomplex I-III activity in permeabilized

905   NSCLC cells stimulated with 10mM pyruvate and 1mM malate following culture in the

906   presence or absence of cystine (n $\geq$3 per condition). **d**, Supercomplex II-III activity in

907   permeabilized NSCLC cells subject to rotenone inhibition of complex I and stimulated with

908   10mM succinate following culture in the presence or absence of cystine (n $\geq$3 per

909   condition). **e**, Immunoblot analysis of PDH complex subunit E2 and α-ketoglutarate

910   dehydrogenase subunit DLST lipoylation following culture in cystine replete or starved

911   conditions. **f**, ACO2 activity in H1299 cells fed/starved of cystine or treated with the iron

912   chelator, DFO (n=3 per condition). **g** and **h**, ETC supercomplex activities in permeabilized

913   H1299 cells following culture in the presence or absence of cystine or treatment with DFO.

914   For all experiments, cells were cultured in treatment conditions for 20 hours prior to the

915   indicated analysis. Data represent mean values ± s.d; n.s., not significant, *, P<0.05, **,

916   P<0.01, ***, P<0.001, ****, P<0.0001. For **b-d**, P values were calculated using two-tailed

917   unpaired Student's *t*-test. For **f-h**, P values were calculated using a one-way ANOVA. All

918   data are representative of at least 3 experimental replicates.

919

41
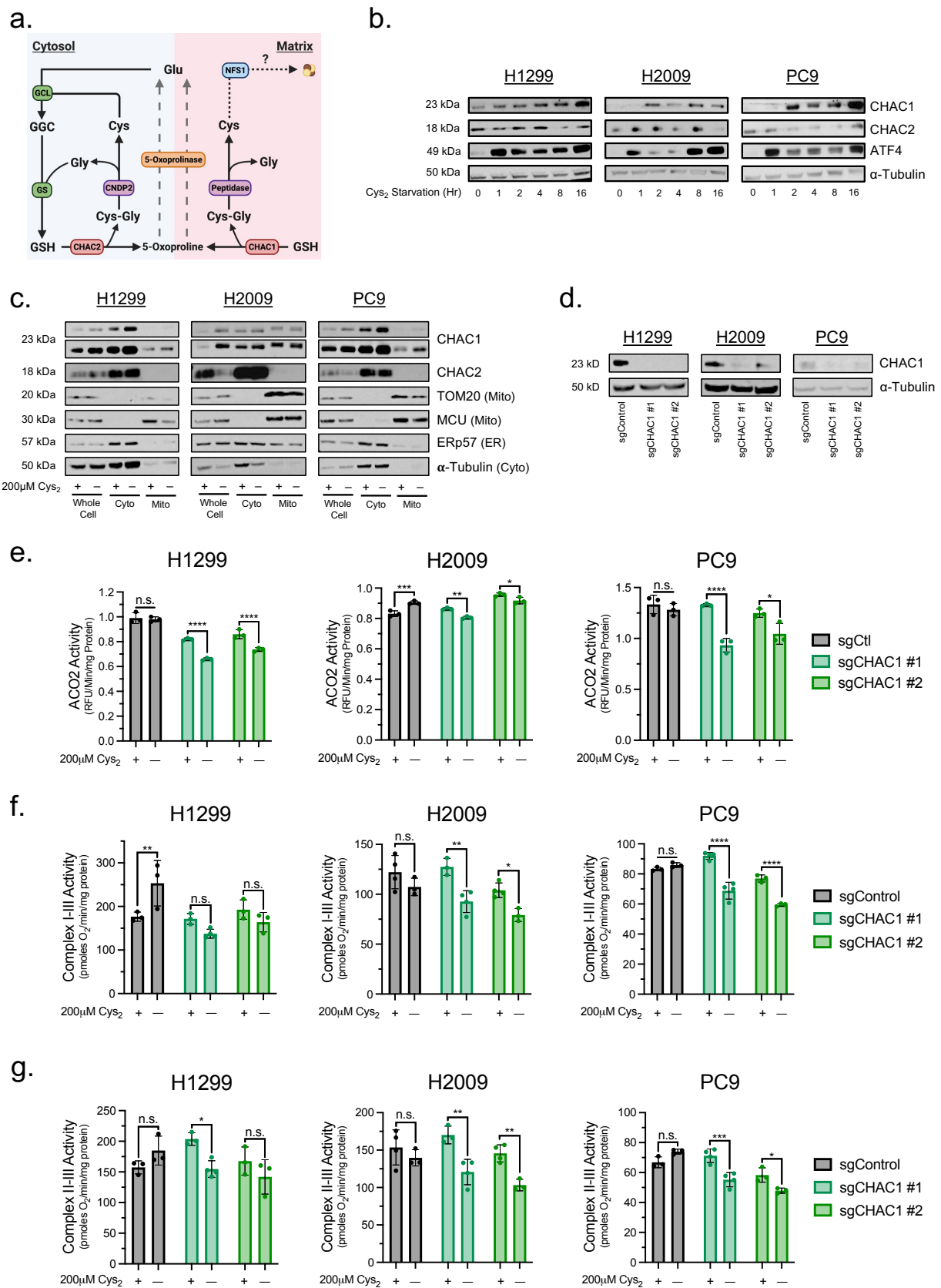
920   **Figure 4**: **CHAC1 Loss Diminishes Fe-S Protein Function Under Cys2 Starvation**. **a**,

921   Schematic of the intracellular GSH cleavage system. **b**, Time-course immunoblot analysis

922   of CHAC1, CHAC2, ATF4, and α-Tubulin expression in H1299, H2009, and PC9 cells

923   under cystine starvation. **c**, immunoblot analysis of CHAC1, CHAC2, ERp57, MCU,

924   TOM20, and α-Tubulin expression in either whole cell lysates or in fractionated lysates

925   upon mitochondrial immunoprecipitation from H1299, H2009, and PC9-HA-Mito cells

926   cultured in the presence or absence of cystine. **d**, immunoblot analysis of CHAC1 and α-

927   Tubulin expression in H1299, H2009, and PC9 cells subject to CRISPR/Cas9-mediated

928   knockout of CHAC1. **e**, ACO2 activities in CHAC1-deficient H1299, H2009, and PC9 cells

929   subject to either cystine replete or starved conditions (n=3 per condition). **f** and **g**, ETC

930   supercomplex activities in permeabilized CHAC1-deficient cells stimulated with their

931   associated substrates following culture in the presence of absence of cystine (n $\geq$3 per

932   condition). For **c**, **e-g**, cells were cultured in the indicated [cystine] for 20 hours prior to

933   analysis. Data represent mean values ± s.d; n.s., not significant, *, P<0.05, **, P<0.01,

934   ***, P<0.001, ****, P<0.0001. For **e-g**, data are representative of at least 3 experimental

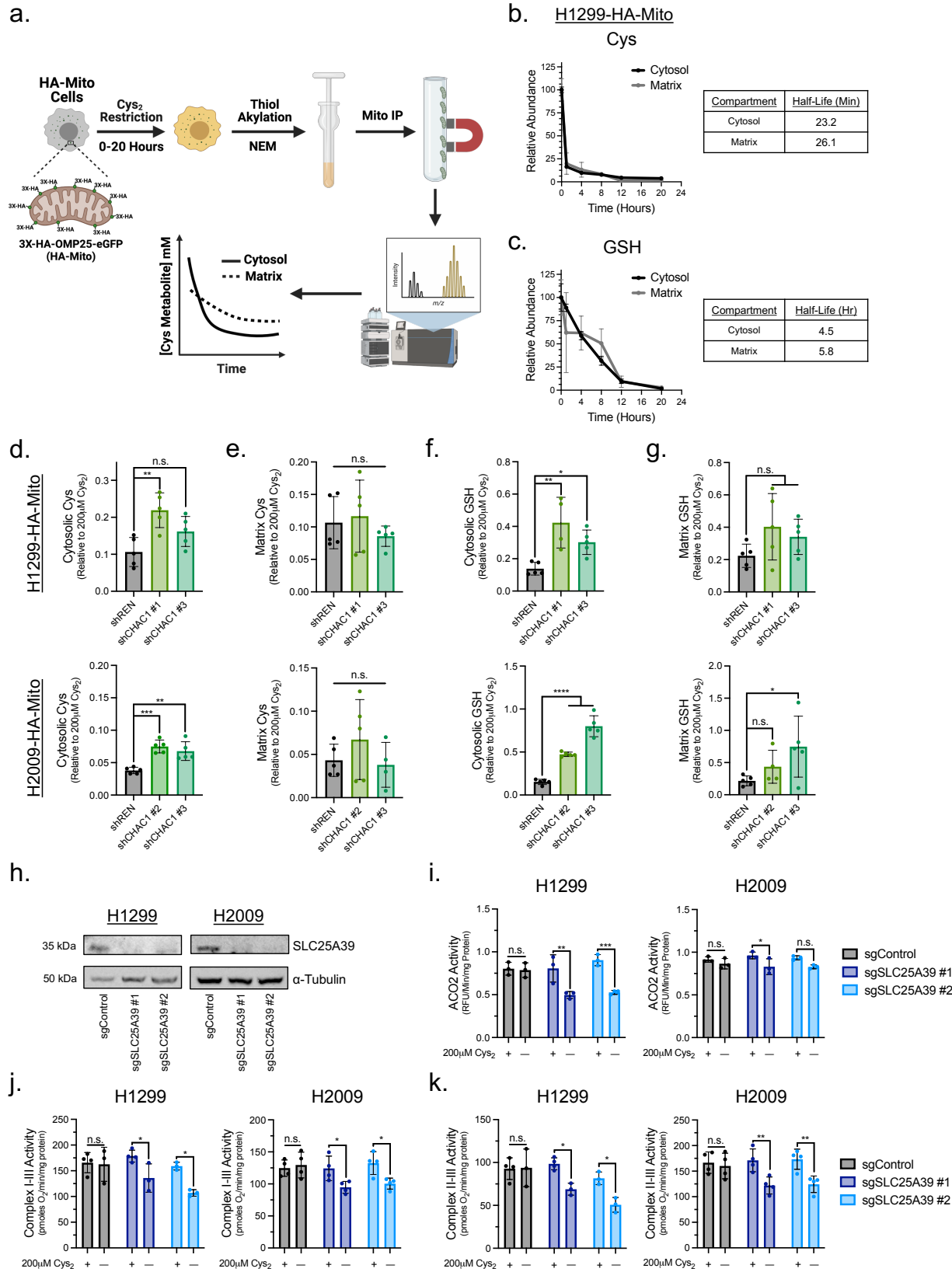935   replicates and P values were calculated using a two-way ANOVA.

936

43

937 **Figure 5**: **CHAC1 Promotes Cellular GSH Depletion Under Cys$_2$ Deprivation**. **a**,

938 Schematic workflow of mitochondrial isolation coupled to LC-MS for the

939 compartmentalized detection of thiol-containing metabolites. **b**, Determination of the half-

940 life of cytosolic and matrix Cys in H1299-HA-Mito cells cultured in the absence of

941 extracellular Cys for 20h (n=3 biological replicates per time point). **c**, Determination of the

942 half-life of cytosolic and matrix GSH in H1299-HA-Mito cells cultured in the absence of

943 extracellular Cys for 20h (n=3 biological replicates per time point). **d-f**, H1299 and H2009-

944 HA-Mito cells were treated with 0.2µg/mL doxycycline for 5 days to induce shRNA

945 knockdown of CHAC1 and then subject to cystine starvation for 12 hours. The pool sizes

946 of **d**, cytosolic Cys, **e**, matrix Cys, **f**, cytosolic GSH, and **g**, matrix GSH were then

947 determined relative to cystine replete conditions (n=5 biological replicates per condition).

948 **h**, immunoblot analysis of SLC25A39 and α-Tubulin expression in H1299 and H2009 cells

949 subject to CRISPR/Cas9-mediated knockout of SLC25A39. **i**, ACO2 activities in

950 SLC25A39-deficient H1299 and H2009 cells subject to either cystine replete or starved

951 conditions (n=3 per condition). **j** and **k**, ETC supercomplex activities in permeabilized

952 SLC25A39-deficient cells stimulated with **j**, 10mM pyruvate and 1mM malate or **k**, 10mM

953 succinate following culture in the presence of absence of cystine (n ≥3 per condition).

954 Data represent mean values ± s.d; n.s., not significant, *, P<0.05, **, P<0.01, ***, P<0.001,

955 ****, P<0.0001. For **i-k**, data are representative of at least 3 experimental replicates and

956 P values were calculated using a two-way ANOVA.

957

44

958
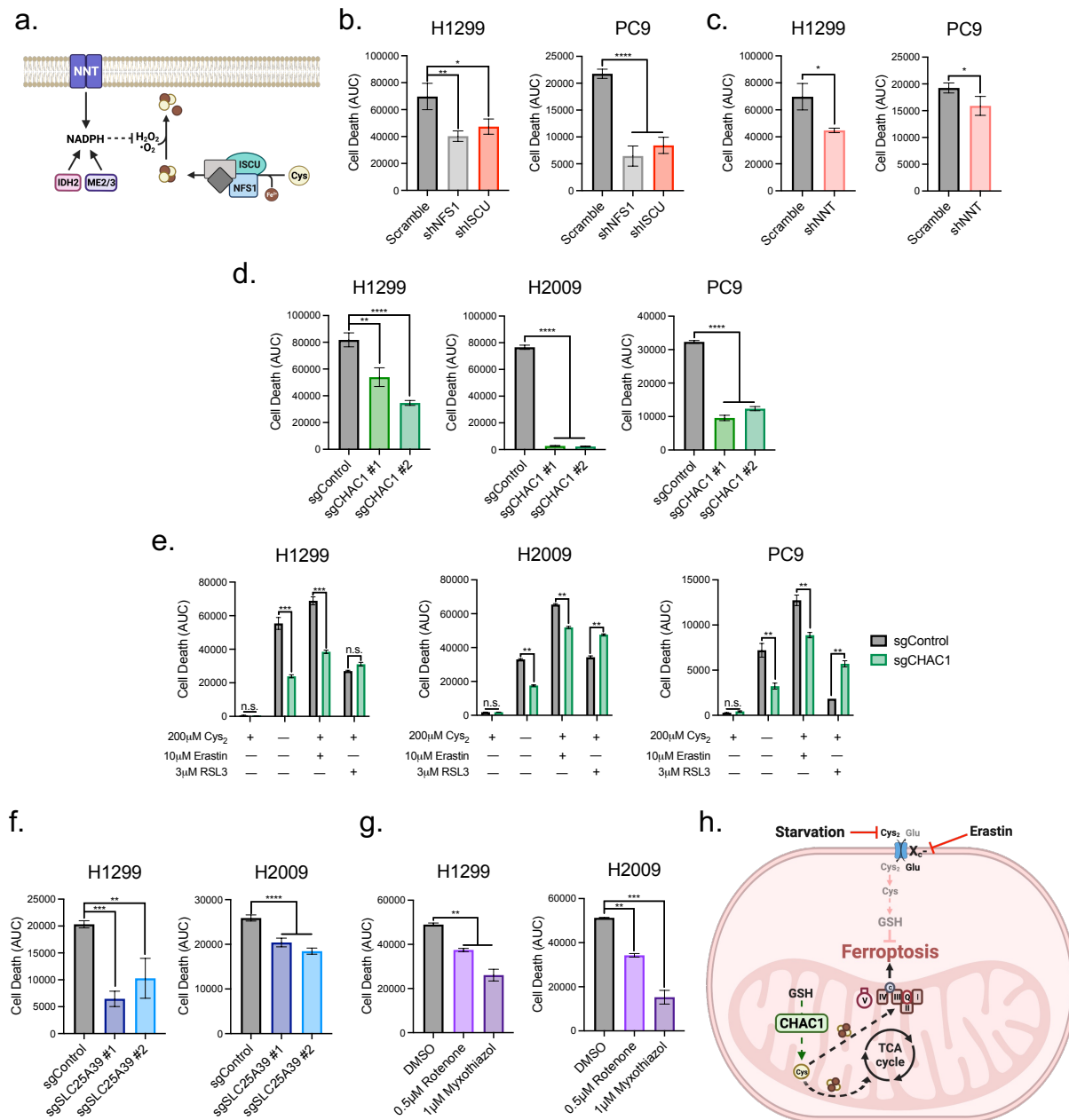
Figure 6: **Mitochondrial Respiratory Function Antagonizes NSCLC Viability in the**

Absence of Extracellular Cys$_2$. **a**, Schematic representation of the two major aspects of

Fe-S cluster homeostasis: *de novo* synthesis and mitigation of cluster oxidation. **b** and **c**,

Quantification of cell death over 48h of cystine starvation in H1299 and PC9 cells following

the disruption of Fe-S cluster homeostasis through shRNA knockdown of **b**, NFS1 and

964   ISCU, or **c**, NNT (n=3 per condition). **d**, Measurement of CHAC1-deficient H1299, H2009,

965   and PC9 cell death under 48h of cystine starvation (n=3 per condition). **e**, Quantification

966   of CHAC1-deficient H1299, H2009, and PC9 cell death over 48h of treatment with

967   indicated inducers of ferroptosis (n=3 per condition). **f**, Determination of cell death in

968   SLC25A39-deficient H1299 and H2009 cells starved of extracellular cystine for 48h (n=3

969   per condition). **g**, Quantification of cell death over 48h in H1299 and H2009 cells subject

970   to ETC inhibition under cystine starvation (n=3 per condition). **h**, Summary schematic

971   depicting that CHAC1 catabolism of GSH supports mitochondrial metabolic function when

972   Cys is limiting to the detriment of NSCLC cell viability. Data represent mean values ± s.d;

973   n.s., not significant, *, P<0.05, **, P<0.01, ***, P<0.001, ****, P<0.0001. For **b-g**, data are

974   representative of at least 3 experimental replicates. For **b-d**, **f** and **g**, P values were

975   calculated using a one-way ANOVA. For e, P values were calculated using a two-way

976   ANOVA.

977

978

979

980

981
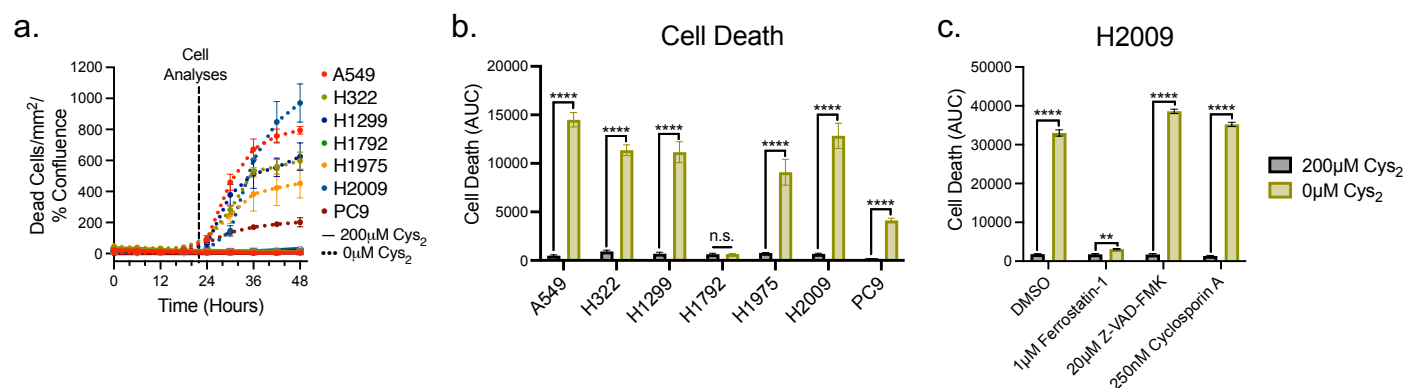
Extended Data Figure 1: **NSCLC Viability is Susceptible to Cys₂ Starvation**. **a**, Plot of the accumulation of dead NSCLC cells over time in cystine replete (solid) or starved (dashed) conditions (n=3 per condition). **b**, Measurement of NSCLC cell death over 48 hours in the presence or absence of cystine. Data represented as area under the curve (AUC) of the plots depicted in **a** (n=3 per condition). **c**, Measurement of cell death over 48 hours in H2009 cells fed/starved of cystine and treated with the indicated inhibitors of ferroptosis (Ferrostatin-1), apoptosis (Z-VAD-FMK), or necroptosis (Cyclosporin A) (n=3 per condition). Data represent mean values ± s.d; n.s., not significant, **, $P<0.01$, ****, $P<0.0001$. For **b**, P values were calculated using a two-tailed unpaired Student's *t*-test. For **c**, P values were calculated using a two-way ANOVA. All data are representative of at least 3 experimental replicates.

47
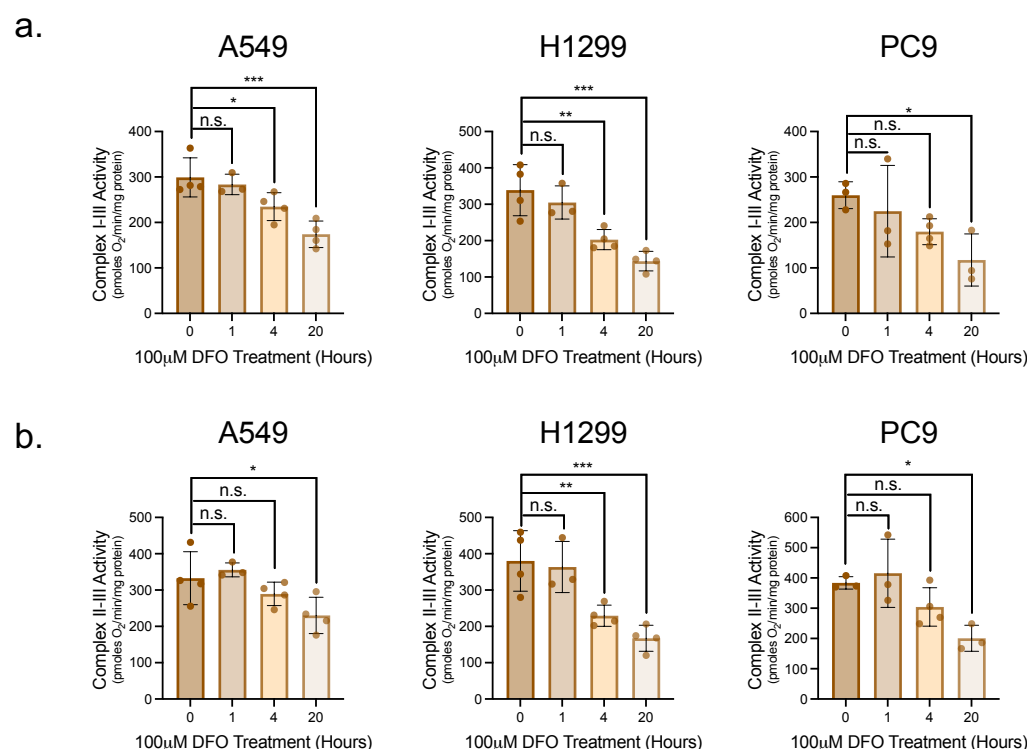
Extended Data Figure 2: **Iron Chelation Promotes a Gradual Loss of Fe-S Protein Function**. **a**, Supercomplex I-III activity in permeabilized A549, H1299, and PC9 cells stimulated with 10mM pyruvate and 1mM malate following treatment with DFO for the indicated time (n ≥3 per condition). **b**, Supercomplex II-III activity in permeabilized A549, H1299, and PC9 cells subject to rotenone inhibition of complex I and stimulated with 10mM succinate following iron chelation for the indicated time (n ≥3 per condition). Data represent mean values ± s.d; n.s., not significant, *, P<0.05, **, P<0.01, ***, P<0.001. For **a** and **b**, P values were calculated using a one-way ANOVA. All data are representative of at least 3 experimental replicates.

48

1004
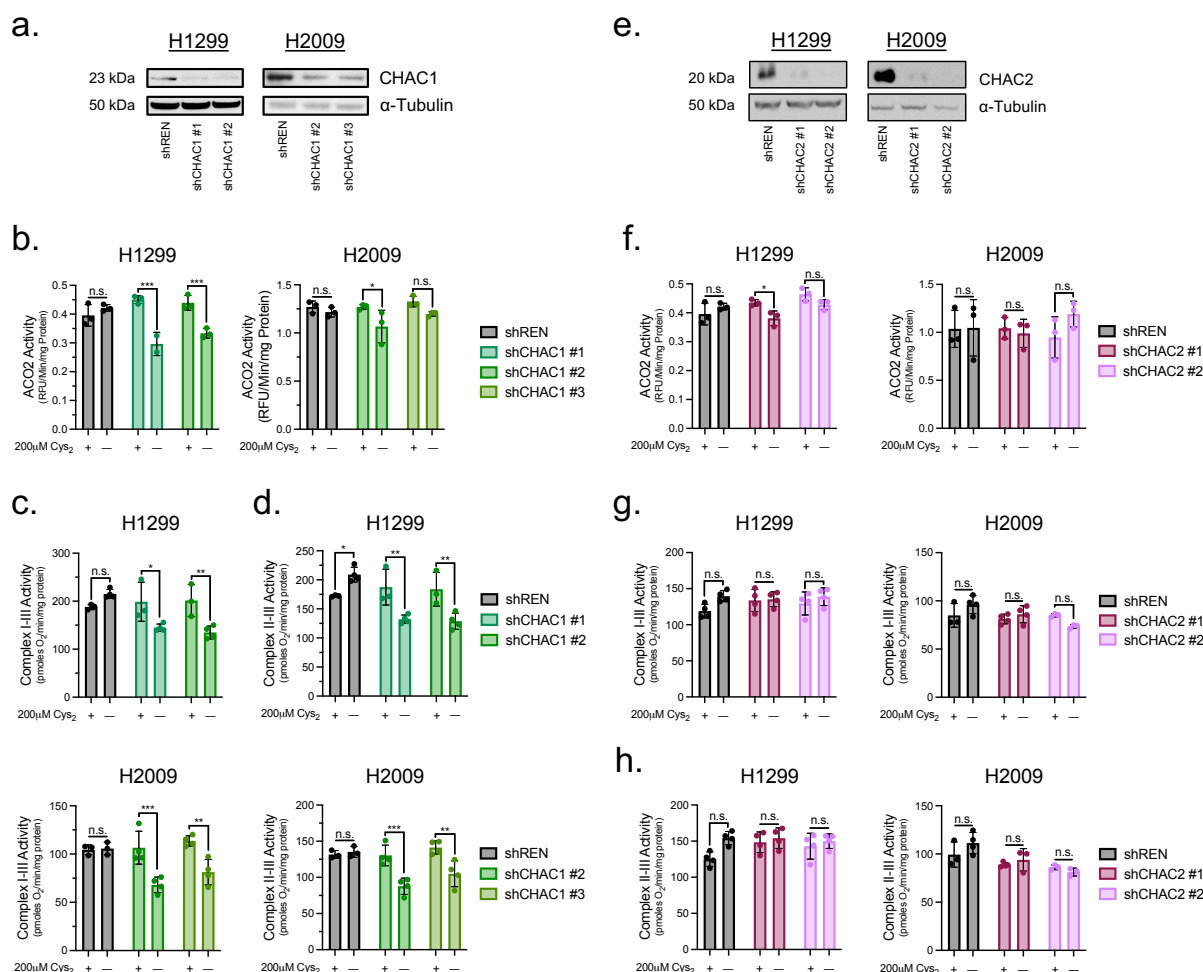
Extended Data Figure 3: **CHAC2 Loss Does Not Influence Fe-S Protein Function**. **a**, immunoblot analysis of CHAC1 and α-Tubulin expression in H1299 and H2009 cells subject to 5-days of 0.2μg/mL doxycycline treatment to induce shRNA-mediated knockdown of CHAC1. **b**, ACO2 activities in H1299 and H2009 CHAC1-knockdown cells subject to either cystine replete or starved conditions (n=3 per condition). **c** and **d**, ETC supercomplex activities in permeabilized CHAC1-knockdown cells stimulated with **c**, 10mM pyruvate and 1mM malate or **d**, 10mM succinate following culture in the presence of absence of cystine (n $\geq$3 per condition). **e**, immunoblot analysis of CHAC2 and α-Tubulin expression in H1299 and H2009 cells subject to 5-days of 0.2μg/mL doxycycline

1014 treatment to induce shRNA-mediated knockdown of CHAC2. **f**, ACO2 activities in H1299

1015 and H2009 CHAC2-knockdown cells cultured in the presence or absence of cystine (n=3

1016 per condition). **g** and **h**, ETC supercomplex activities in permeabilized CHAC2-

1017 knockdown cells stimulated with their associated substrates following culture in cystine

1018 replete or starved conditions (n $\geq$3 per condition). For **b-d**, **f-h**, cells were treated with

1019 0.2μg/mL doxycycline for 5 days prior to analysis and cultured in the indicated [cystine]

1020 for the final 20 hours. Data represent mean values ± s.d; n.s., not significant, *, P<0.05,

1021 **, P<0.01, ***, P<0.001, ****, P<0.0001. For **b-d, f-h**, data are representative of at least

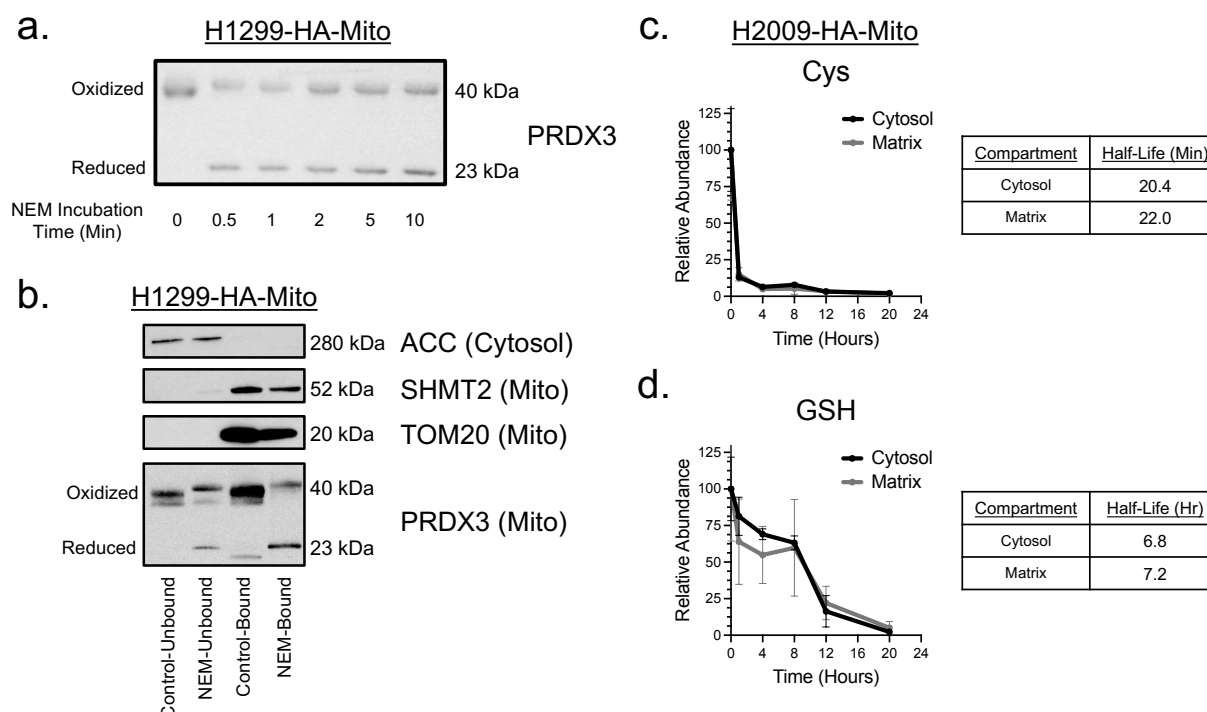1022 3 experimental replicates and P values were calculated using a two-way ANOVA.

1023

1024

1025

1026

1027

Extended Data Figure 4: **Cys$_2$ Starvation Promotes a Rapid Depletion of Intracellular Cys**. **a**, Redox immunoblot determination of reduced PRDX3 stabilization in H1299-HA-Mito cells treated with 25mM NEM for up to 10 minutes prior to mitochondrial immunoprecipitation. **b**, Immunoblot analysis of ACC, PRDX3, SHMT2, TOM20 expression in H1299-HA-Mito cells following mitochondrial immunoprecipitation ± a 1 minute incubation with 25mM NEM prior to mitochondrial isolation. **c**, Determination of the half-life of cytosolic and matrix Cys in H2009-HA-Mito cells cultured in the absence of extracellular Cys for 20h (n=3 biological replicates per time point). **d**, Determination of the half-life of cytosolic and matrix GSH in H2009-HA-Mito cells cultured in the absence of extracellular Cys for 20h (n=3 biological replicates per time point). Data represent mean values ± s.d.
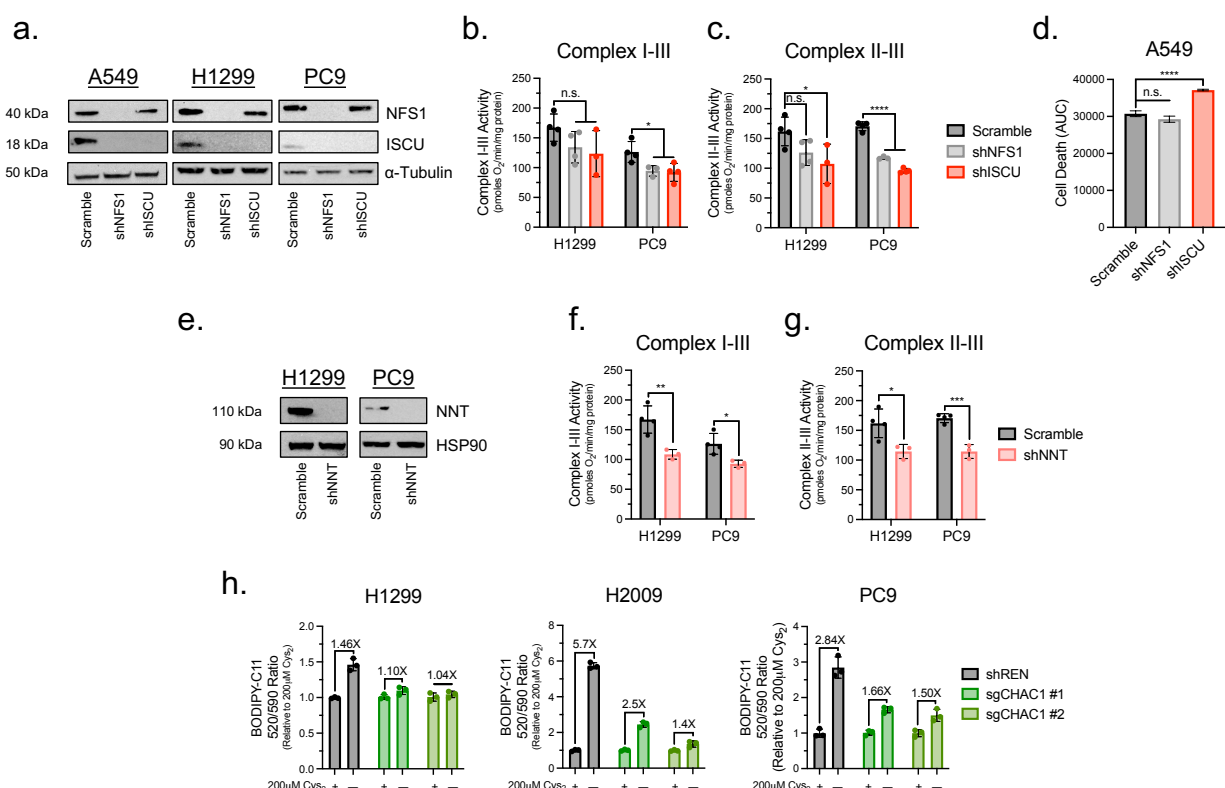
Extended Data Figure 5: **Fe-S Protein Function is Diminished Upon Disruption of Fe-S Cluster Homeostasis**. **a**, Immunoblot analysis of NFS1, ISCU, and α-Tubulin expression in A549, H1299, and PC9 cells 4d post-infection with scramble, shNFS1, or shISCU lentivirus. **b** and **c**, ETC supercomplex activities in permeabilized H1299 and PC9 cells stimulated with **b**, 10mM pyruvate and 1mM malate or **c**, 10mM succinate 4d post-infection with scramble, shNFS1, or shISCU lentivirus (n $\geq$3 per condition). **d**, Quantification of cell death over 48h of cystine starvation in A549 cells following the disruption of Fe-S cluster synthesis through knockdown of NFS1 and ISCU (n=3 per condition). **e**, Immunoblot analysis of NNT and HSP90 expression in H1299, and PC9 cells 4d post-infection with scramble or shNNT lentivirus. **f** and **g**, ETC supercomplex activities in permeabilized H1299 and PC9 cells stimulated with their associated substrates 4d post-infection with scramble or shNNT lentivirus (n $\geq$3 per condition). **h**,

1053   Relative BODIPY-C11 fluorescence ratio of CHAC1-deficient H1299, H2009, and PC9

1054   cells cultured in the presence or absence of cystine for ≥20h as an indicator of the extent

1055   of cellular lipid peroxidation (n=3 per condition). Data represent mean values ± s.d; n.s.,

1056   not significant, *, P<0.05, **, P<0.01, ***, P<0.001, ****, P<0.0001. For **b-d,** P values were

1057   calculated using a one-way ANOVA. For **f** and **g**, P values were calculated using a two-

1058   tailed unpaired Student's *t*-test**.** Data are representative of at least 3 experimental

1059   replicates.